



Rapid Solution Exchange to Neuronal Culture Grown on Multi Electrode Arrays

by Nitzan Herzog

Thesis submitted to The University of Nottingham
for the degree of Doctor of Philosophy, January 2017

Contents

List of Figures	5
Abstract	7
Acknowledgements	8
1 Introduction	9
1.1 The MEA culture model for network activity in neuronal ensembles	9
1.1.1 Notable achievements of the neuronal culture on MEA model	9
1.2 Volume transmission in neuroscience	9
1.2.1 Neuromodulator transmission and plasticity	9
1.3 Microfluidics for cell culture	9
1.3.1 Rapid drug delivery	9
1.3.2 Microfluidics in neuroscience	10
1.3.3 Neurons and flow	10
1.4 Ph.D objectives	10
2 Methods	11
2.1 Basic fabrication elements	11
2.1.1 PDMS preparation	11
2.1.2 Thin film spinning	11
2.1.3 Soft lithography	11
2.1.4 PDMS extraction	11
2.2 Bonding techniques	12
2.2.1 Plasma bonding	12
2.2.2 Double sided silicone tape	12
2.3 Surface coating	13
2.3.1 Open surface	13
2.3.2 Devices - Bond-then-PLL	13
2.3.3 Devices - PEI-then-bond	13
2.4 Seeding and maintaining of Neuronal cultures	13
2.5 MEA recording and stimulation	13
2.5.1 Spike detection and noise removal	13

2.5.1.1	Automatic quantification of active channels	13
2.5.2	Electrical stimulation	14
2.5.2.1	Automatic detection of responsive channels	14
2.5.3	Correlation maps	14
2.5.4	Burst detection	14
2.5.5	Functional connectivity analysis	14
2.6	Plasticity protocol	18
2.7	Conditioned media production	18
2.8	Flow experiments	18
2.8.1	Heated chamber	18
2.8.2	Steady flow	18
2.8.3	Pulsing	19
2.9	Immunohistochemistry	20
3	Establishment of a culture model for network activity in neuronal ensembles	21
3.1	Introduction	21
3.2	Development of spontaneous activity in Mouse cultures	22
3.2.1	Statistics of activity and synchronicity measures	25
3.2.2	Comparison between mouse and rat cultures	29
3.3	Evoked activity	30
3.4	Plasticity induction in the presence of dopamine	33
3.4.1	Examining changes in response to stimulation	35
3.4.2	Examining changes in functional connectivity	39
3.5	Chapter conclusion	41
4	Viability of neuronal cultures in microfluidic devices in static conditions and under flow	43
4.1	Introduction	43
4.2	Long term neuronal cultures in microfluidic devices	45
4.2.1	Development of protocol	45
4.2.1.1	Evaporation and surface chemistry considerations	46
4.2.1.2	Considerations of factor circulation	47
4.2.1.3	Alternative bonding methods	51
4.2.1.4	Extraction of PDMS	52
4.2.2	Growing microcultures in plasma bonded devices	55
4.3	Viability of neuronal cultures under steady microfluidic flow	59
4.3.1	Pilot flow study	59
4.3.2	Quantitative viability analysis	61
4.4	Chapter conclusion	66

5 Activity Under Microfluidic Flow	67
5.1 Neuronal cultures in cross flow devices on MEAs	67
5.2 Activity under flow for young cultures	68
5.2.1 Effect of flow rate	68
5.2.2 The microwells approach for shear reduction (optional)	68
5.2.3 The semi-permeable membrane approach for shear reduction	68
5.2.3.1 The shifted membrane paradigm (optional)	69
5.2.4 Effect of old conditioned media	69
5.2.5 Considerations of diffusive flux	69
5.3 Activity under flow for old cultures	74
5.3.1 Effect of age under fast flow	74
5.3.2 The effect of the media	74
5.3.3 Stability of spontaneous motifs (optional)	74
5.3.4 Does flow disrupt the synaptic function?	74
5.4 Putative mechanism to explain the observed results	77
5.5 Chapter conclusion	77
6 Rapid Programmatic Drug Delivery to a Neuronal Microculture	78
6.1 Pulsing performance in microculture devices	78
6.1.1 Analysis of pulsing visualized by fluorescein	79
6.1.2 Numerical simulation of drug pulsing	79
6.1.3 Effect of well depth on pulsing performance (optional)	79
6.2 Establishment of long term Neuronal microcultures	82
6.2.1 PEI-then-all-tape devices	82
6.2.2 PEI-then-PDMS-tape device	82
6.2.3 Activity in normal conditions	82
6.3 Behaviour under flow	86
6.4 Glutamate pulsing	86
6.5 Dopamine pulses	87
7 Discussion	92
7.1 The utility of the culture model	92
7.2 The shear protection vs. conditioning protection issue	92
7.2.1 Limitation uncovered by the conducted experiments	92
7.2.2 Avenues for further expansion of the model	92
7.3 Importance of extrasynaptic environment	92
7.4 Prospects of the <i>in vitro</i> volume transmission model	93

A Appendix	94
A.1 MEA Data sheets	94
A.2 Heat transfer for water flowing in a PTFE tube	94
Bibliography	94

Chapter 3

Establishment of a culture model for network activity in neuronal ensembles

3.1 Introduction

As reviewed in section 1.1, neuronal cultures grown on multi electrode arrays have emerged as a successful model for studying generic properties of neuronal ensembles at the network level. The overall purpose of this Ph.D work is to provide this model system with an added functionality of phasic volume transmission, thus achieving a novel experimental platform for studying how fine temporal feature of extrasynaptic agonist concentrations interact with the activity. In this first chapter we describe the establishment of the standard neuronal cultures on MEA model system within our laboratory group. We followed their development for over 3 weeks *in vitro* and demonstrated that they develop normally and exhibit hallmark network activity, both spontaneous and evoked, and comply in characteristics with the literature gold standard.

To date, MEA investigation have been dominated by use of primary cultures derived from rat. However, mouse is generally a more popular neuroscience model and offers a by far greater library of molecular and genetic tools so using it as a tissue source might be beneficial. Thus, an additional contribution presented in this chapter is the examination of mouse based cultures and comparison with rat preparations in the context of MEA investigations. We found that the mouse cultures were difficult to culture on the MEA surface and exhibited a delayed synaptic maturation as compared to their rat counterparts. Nevertheless, mouse cortical cultures that were able to develop exhibited all the richness of network phenomena described in rat literature.

Finally, prior to engaging in the development of the microfluidics system for rapid pulsing

we took the chance to explore generating a slower phasic dopamine signalling model in these traditional experimental systems by manually pipetting the agonist (in this case dopamine) onto the culture followed by replacement of the media. We used this approach to revisit the long standing issue of plasticity in these systems.

Synaptic plasticity without neuromodulation in neuronal cultures on MEA has been controversial as multiple reports produced contradictory or negative results (reviewed further in section 3.4). This in contrast to slices and *in vivo* systems where activity dependent plasticity induced through stimulation or behavioural paradigms is well established [1]. It should be noted that spike timing dependent plasticity had been demonstrated in hippocampal cultures for pre and post synaptic neuron pairs explicitly controlled and monitored via patch clamp [2]. The lack of success on MEAs cannot, therefore, be attributed so a skewed biology of neurons in culture and it is not yet clear if it is related to the poorer sensitivity of the extracellular recordings (sensitive only to super-threshold processes), to the culture network topology which needs to be accounted for in the stimulation protocols, or to the absence of neuromodulators. Indeed that dopamine modulates plasticity in culture has been established but using bath application therefore only interrogating tonic effects [3, 4].

Thus, as a final step in this chapter, we revisited the question of plasticity induction and found that a standard tetanization protocol does not produce a measurable change in evoked responses or in functional connectivity in our cultures. We then explored whether slow pulsing of dopamine by manually adding it during the plasticity-induction phase (tetanization) and washing it away immediately after could have an enabling effect on plasticity. We found that the altered protocol results in a change to activity and connectivity measures but argue that the effect of the washing cannot be easily separated from that of the dopamine, hence confusing the interpretation. This chapter thus serves to establish the multi electrode array electrophysiology technique and to provide motivation for the development of the microfluidics technology in the following chapters.

3.2 Development of spontaneous activity in Mouse cultures

Primary mouse embryonic cortical cultures were seeded on pre-coated MEAs as described in sections 2.3 and 2.4. All MEAs used for the work undertaken in this chapter are of 8x8 configuration with $30\mu m$ electrodes and $200\mu m$ electrode spacing (see appendix A.1 for data sheets).

Figure 3.1 A-C shows microscope images of a representative culture over 18 days in culture. The images show how over the first few days the cells became polarized and extended neurites and dendrites. As these continued to grow, branch and generate synaptic contacts the culture obtained a weblike appearance. In later days of development an obvious mass of extracellular tissue was evident in between the cells covering the previously bare glass

and engulfing the fine cellular processes. In the case of the mouse cultures, many of the preparations did not develop properly whereby, despite good initial adhesion, the majority of the plated cells did not continue differentiating and after a few days detached from the surface and degenerated (figure 3.1 D). This was the case for over half of plated cultures and these were discarded from the experiment. Cultures prepared from rat embryos did not present this sort of inconsistency and generally developed at a high success rate despite using the same MEAs and generally same coating and seeding procedures.

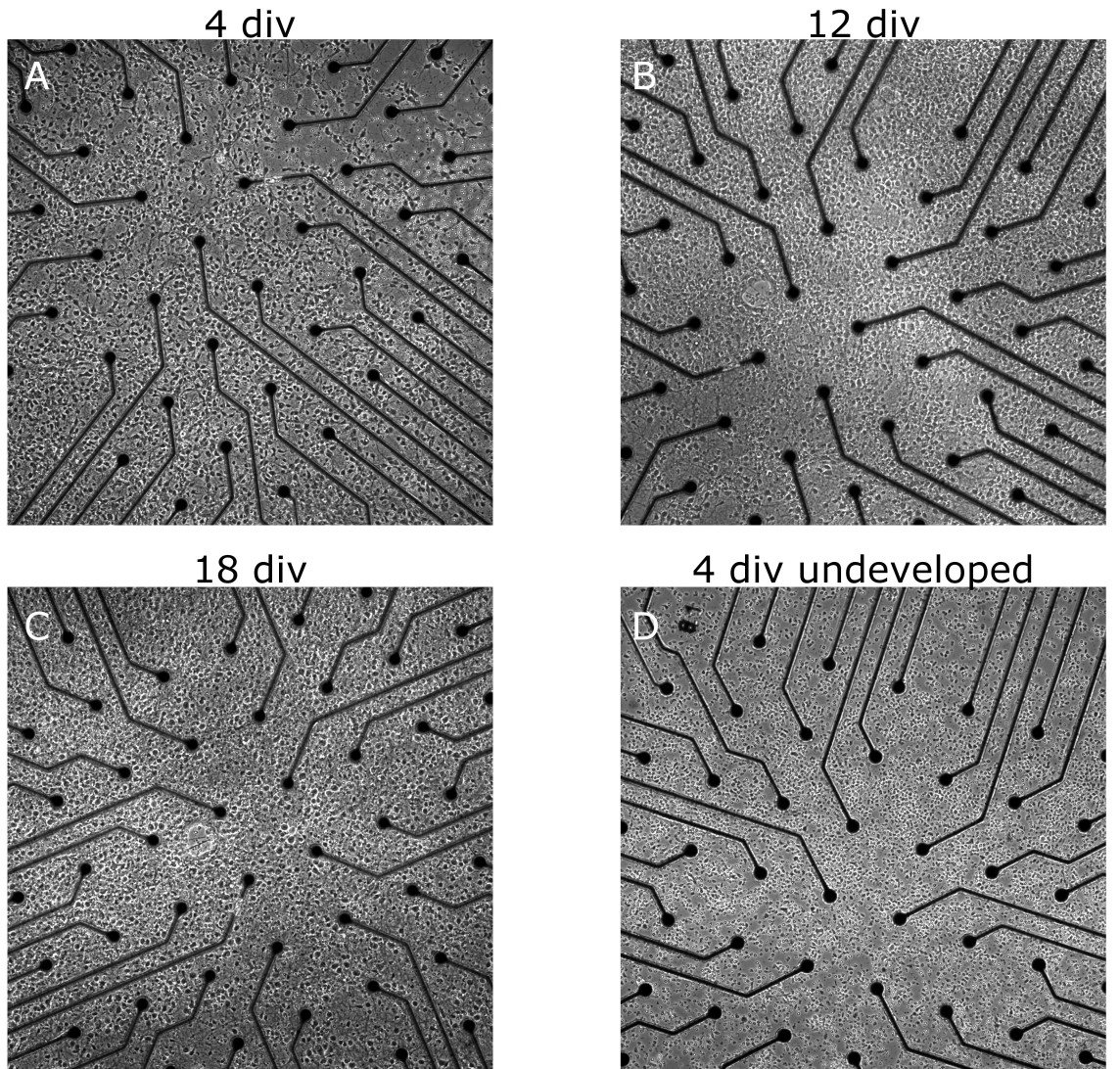


Figure 3.1: Cortical mouse cultures develop and become a densely interconnected neural tissue. (A-C) Cortical culture prepared from mice embryos and plated on micro-electrode arrays imaged on several time points over development. by 4 days *in vitro* most of the cells show an obvious polarized neuronal morphology and extend neurites. At 12 days *in vitro* a thick ECM tissue is evident between the cells (D) Example of a seeded culture that didn't show proper development. The electrodes are $30\mu m$ wide and spaced $200\mu m$ apart.

We monitored the activity of the mouse cultures for 3 weeks in *in vitro*. The analysis

performed throughout this thesis is restricted solely to spiking activity and lower frequencies associated with local field potentials were filtered out of the data. Spike detection was performed through a combination of match filtering and simple threshold crossing. A second pre-analysis step detected and removed erroneous spike waveforms induced by electromagnetic noise and which generated synchronized spiking events across several channels (see section 2.5 for full description of the pre-analysis). No spike sorting was attempted as this was shown to be ineffective in culture [5].

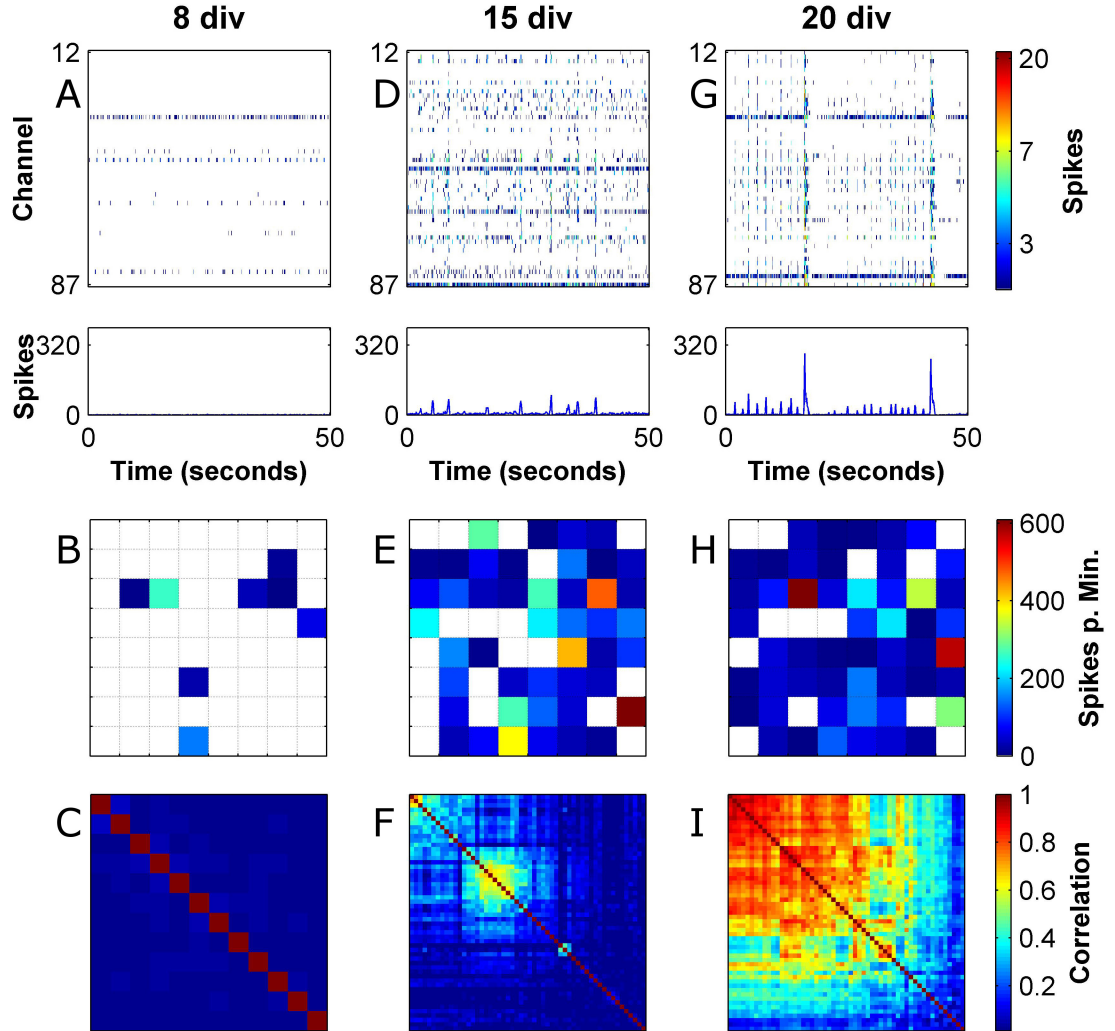


Figure 3.2: Spontaneous activity in mouse culture develops from tonic firing into synchronized bursting events. (A,D,G) Raster plot of spontaneous activity in mouse culture in 3 developmental time points exhibiting the change in the activity structure. Rasters plots are presented in 100ms bins. Bottom panels show summation of raster over all channels. (B,E,H) Activity maps showing the spatial organization of activity on the MEA in the same time points. (C,F,I) Dendrogram- sorted correlation matrices showing groupings of channels into correlated blocks.

Virtually no spikes were recorded until approximately 5 days *in vitro*, at which point tonic firing started to emerge in some of the channels. Beyond this point, the proportion of active channels and measured activity increased until reaching a plato at about 13 days *in vitro* (figure 3.3). The development of synchronization in the cultures is exemplified in Figure 3.2 which shows raster plots at several developmental stages along with the associated mean firing rate maps and dendrogram-ordered cross channel correlation matrices. At 8 days *in vitro* only a small proportion of the channels was tonically active and showed regular spiking (figure 3.2 A). At this point there was very little correlation across the channels suggesting that the measured spike trains aren't driven by synaptic integration but rather controlled through intrinsic neuronal excitability. At 15 days *in vitro* most of the MEA channels exhibited spiking activity (figure 3.2 D). At this point some correlated spiking events (network bursts) began to emerge although most of the the activity was still regular and uncorrelated. These network bursts were not easily discernible in the multi channel raster plot but were evident as large peaks in the summated network activity and as increased correlations between a subset of the channels. To appreciate the significance of the observed correlations, we generated surrogate independent spike rasters where the spikes trains were drawn from an independent Poisson processes with rate parameters as in the original channels (see section 2.5.3). For the data shown in figure 3.2, the maximal observed correlations between two different channels in the surrogate independent spike rasters were 0.05, 0.05 and 0.07 for 8, 15 and 20 days *in vitro*, respectively. These values are negligible compared to the observed values in the correlation matrices for 15 and 20 days *in vitro* and therefore indicate a genuine coupling between the measured neurons. Towards the end of the 3rd week (here 20 days *in vitro*) most of the activity in the cultures was restricted to the network bursts (figures 3.2 G and 3.4 E).

During the early phases of synchronicity (beginning of 3rd week, here 15 days *in vitro*) it was common to observe more than one synchronized cluster of channels in the dendrogram-sorted correlation matrices (figure 3.2 F). Nevertheless, correlations between these clusters continued to develop to the point where the entire culture became a single synchronized unit (end of 3rd week, figure 3.2 I). Previous work showed that applying synaptic blockers at non saturating quantities to fully developed neuronal cultures reveals an underlying modular connectivity pattern through breaking the weaker links between modules while still preserving denser intra-module connections [6]. Our results are compatible with this notion of underlying modularity and show that the modules are formed at the earlier stages of synaptic maturation.

3.2.1 Statistics of activity and synchronicity measures

Figure 3.3 shows activity related statistics over our experimental data set comprising 5 mouse cultures. Long term electrophysiological studies of this type have been facilitated by the introduction of the MEA technology which easily allows sampling of multiple cells

in parallel and repeatedly over long stretches of time. Patch clamp electrophysiology, in contrast, is usually restricted to a few cells at a time and cultures have to be discarded after a single experimental session as it is harder to maintain the cells healthy and sterile. Nevertheless, MEA developmental studies have been almost completely exclusive to cortical cultures made from rat embryos. Thus, with this study, apart from ascertaining that the cultures are healthy, we examine if there are any developmental differences between mouse and the rat based preparations.

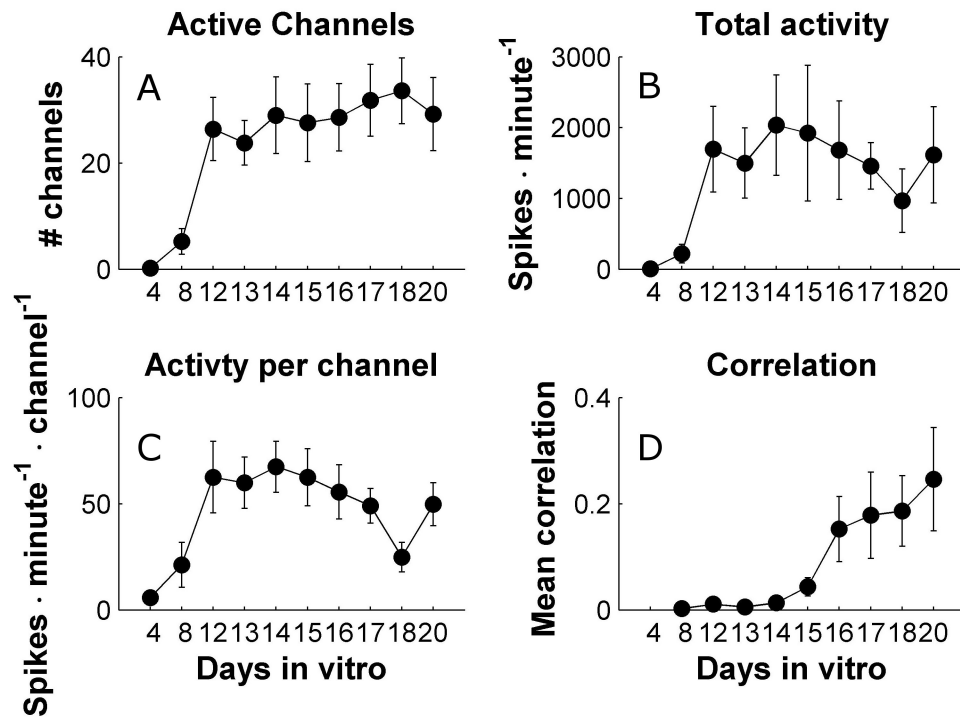


Figure 3.3: Development of synchronicity in mouse cultures lags after activity. (A) Development of the number of active channels as a function of culture age. (B) Development of the total number of spikes recorded on all MEA electrodes. (C) Development of the mean neuron firing rate (average of firing rate over active channels - implied assumption that each electrode records a single neuron). (D) Development of mean correlation. Mean correlation for a recording is the average of the correlation matrix taken without the diagonal. The data is shown as mean and SEM based on n=5 cultures.

The cultures do not become fully active until approximately 2 weeks in culture suggesting that this period of time is required for the seeded progenitor cells to become mature excitable neurons (figure 3.3 A-C). This time frame for activity onset is consistent with rat literature [7, 8, 9] and is generally accepted with regard to culture electrophysiology. After the initial increase, the firing rates (figure 3.3 C) stabilize at around 1Hz and don't exhibit a time dependent trend (1-way ANOVA, p=0.3). The average firing rate per channel is compatible with studies from rat cultures which reported values in the range of 0.4 – 1.5Hz [9, 7, 10, 11]

but the lack of trend is strikingly different as rat cultures are reported to show a marked increase in individual firing rates until 21 days and a decline afterwards [9, 12].

Figure 3.3 D shows the development of correlations in our cultures. The correlation value for a given recording is the mean of the correlation matrix (e.g., figure 3.2 C,F and I) without the diagonal. Evidently, despite the stabilization of the mean unit firing rates at day 13 *in vitro*, significant correlations started to arise only from about 17 days *in vitro*. This suggests that the excitability in the cultures is initially controlled by intrinsic homeostatic mechanisms which are later replaced by synaptic drive. Remarkably, the apparent increase in synaptic efficacy is not accompanied by an increase in spiking activity suggesting that the unit mean firing rate of 1Hz is a controlled quantity which the neurons maintain in the face of a changing network environment around them. Indeed, it has been shown that cultured neurons are capable of rapidly modifying their intrinsic excitability in response to pre-synaptic blockers [11].

To further characterize the spontaneous activity in the cultures we employed a burst detection algorithm as detailed in section 2.5.4 and extracted parameters of burst related measures, shown in figure 3.4. Not surprisingly, the development of bursting activity followed the same pattern as mean correlation and trailed the development of activity by a few days (figure 3.4 A,D compared to figure 3.3 A-C). This separation between measures of pure activity and of those of synchronicity underlines the utility of the MEA system in recognizing and disentangling biological processes that are linked. Previous rat cultures studies report that regular bursting is apparent already towards the end of the 2nd week *in vitro* [7, 8, 9, 12] whereas in our mouse data this was rare. In these reports the evolution of bursts appeared to go hand in hand with the evolution of activity, both of which peaked at 21 days *in vitro* and declined afterwards. As bursting behaviour in our data is a few days delayed and starts in the middle of the 3rd week *in vitro* it is plausible that a similar trend (but delayed) would be observed had we recorded further into the 4th week.

It should be noted that the peak burst rate value observed (15 minute⁻¹) was much higher than the one reported for rat cultures at the same age of development (5 minute⁻¹) [9]. However, we do not believe that this strong discrepancy lies in the difference between the preparations. Rather, our burst detection algorithm (section 2.5.4) uses an innovative approach for identifying synchronized events. Our method computes surrogate spike rasters with identical firing rates as the original data but without correlations to define the burst detection threshold. The thresholds defined in this way are likely to be tighter than for previous approaches where the thresholds were manually selected based on personal preference of how well they fit the data [8, 13]. Since our thresholds are based on an objective criteria we argue that the observed burst rate indeed reflects synchronized events and that the rate of these is actually greater than previously reported.

Further evidence for delayed synaptic maturation is provided by the burst width and burst size measures. Previous work have established that bursts in naive rat cultures exhibit

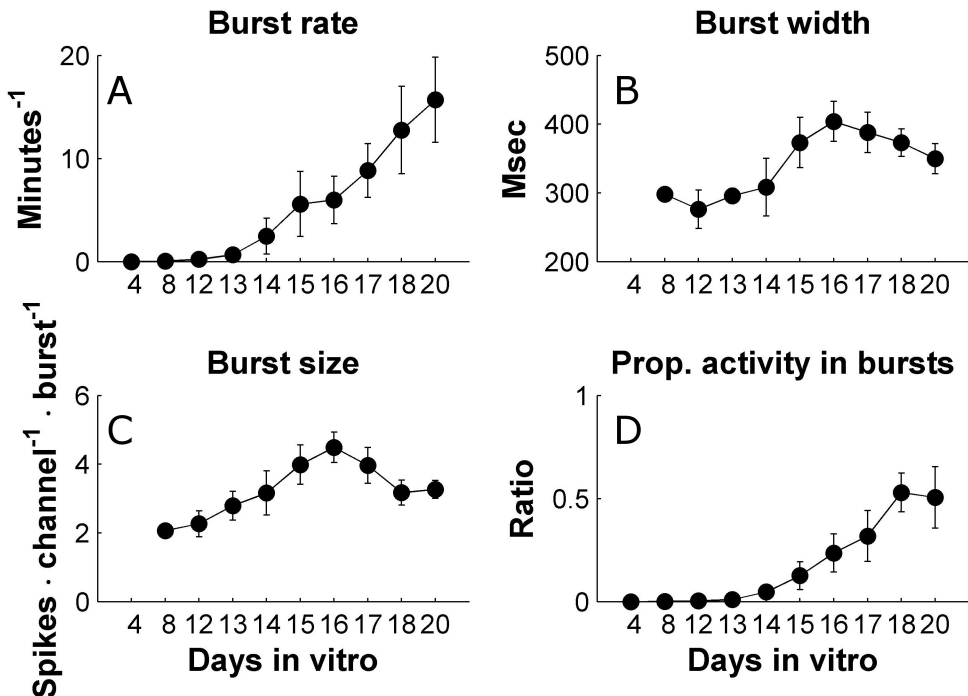


Figure 3.4: **Development of bursting measures in mouse cultures lags behind activity.** (A) Development of burst rate as a function of culture age. (B) Development of burst width. (C) Development of burst size. (D) Development if the ratio between the number of spikes observed with in bursting events and the total recorded spikes. Data is shown as mean and SEM based on n=5 cultures.

wide temporal profiles with long tails of spike discharges that could last up to several seconds [9, 14]. Over the 3rd-4th weeks the burst profiles become narrow and exhibit increasingly faster termination until saturating in the end of the 4th week. This change is attributed to the development of the GABAergic neurotransmission which was shown to occur 1-2 weeks in delay as compared to the glutamatergic system [15]. Hence it has been postulated that feedback loops operating through inhibitory interneurons become functional only in the aforementioned time period [7]. In the rat data the bursts show maximal width when they first appear (10-14 days *in vitro*). In our data, a similar trend is observed with peaks appearing in the burst size and burst width measures at 17 days *in vitro*, which is approximately the point when bursting activity became appreciable (time effect was found significant through 1-way ANOVA for both burst size and burst width measures with p=0.035 and 0.028, respectively).

Taken together, the results from the spontaneous activity study demonstrate that, on one hand, the development of neurotransmission and synaptic connections in our mouse cultures appears to be delayed between 3 days to one week. On the other hand, irrespective of the delay, the cultures exhibit all the activity features expected from literature, such as,

homeostatic control of excitability, underlying modularity and development of synchronicity and bursting activity which evolve in accordance with the development of the synaptic networks. Nevertheless, as mentioned in the beginning of this section, the mouse cultures posed an added difficulty of a high culturing failure rate which, together with the delayed electrophysiological development raised concerns regarding their utility and ease of use. We therefore decided that, following the study performed in this chapter, rat based preparations would be used for the remainder of the Ph.D work. The next section will outline a brief pilot study to compare our rat based preparations with the mouse based ones and assert that the former shows an electrophysiological profile in par with the literature.

3.2.2 Comparison between mouse and rat cultures

In order to compare the functional development of mouse based and rat based cultures we recorded spontaneous activity from a set of rat cultures, prepared using a protocol identical to the mouse ones. It should be noted that although the reagents, dissociation techniques and growth conditions were indeed identical, there was still a difference originating from the differing tissue source. The rats were delivered from a private animal facility and operated on within our lab space, whereas the mice were bred in a university based animal facility where they were also operated. The cell suspension for the mice culture therefore had to be carried between buildings before plating which could account for any observed differences. Nevertheless, we believe this to be unlikely.

Figure 3.5 shows a comparison between rat based and mouse based cultures at the same age *in vitro* for several activity and synchronicity measures introduced earlier. A particularly pronounced difference was observed in the closely related measures of correlation and ratio of intra-burst to total activity both of which showed a significantly higher values in the rat cultures (1-sided unbalanced t-test, $p=0.017$ and 0.039 , respectively). These difference demonstrate that mouse cultures exhibited more uncorrelated activity as compared with their rat counterparts. This reiterates the observation discussed in the previous section that the mouse cultures show delayed synaptic development.

Another observed difference is that the mouse cultures showed a significantly higher average unit firing rate (one sided unbalanced t-test, $p=0.048$). This result could be another manifestation of the rat neurons being more attuned to the synaptic drive from the network but is harder to interpret. In any case, the mean values for both preparations types (1Hz and 0.5Hz for mouse and rat, respectively) are within the literature range ($0.4 - 1.5\text{Hz}$).

Both preparations showed a nearly identical burst rate of about 15 minute^{-1} . The burst rate measure is different to the correlation and activity ratio measures in that it counts synchronized events but is indifferent to activity outside such events. This in contrast to the correlation and intra-burst to total spikes ratio measures which are sensitive to activity both inside and outside the synchronized events. The fact that the reduced synaptic coupling in mouse cultures does not affect the burst rate suggests that the this measure is strongly

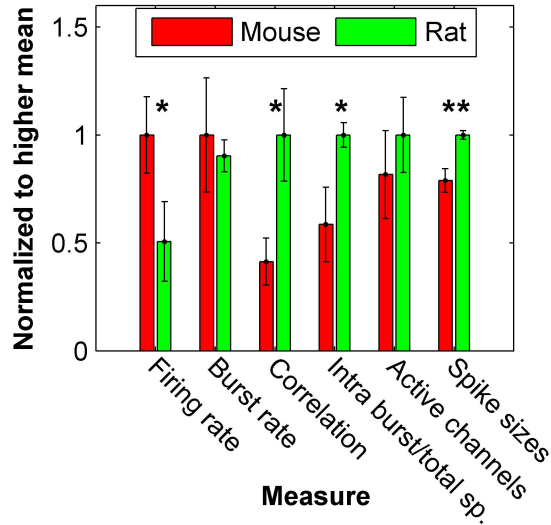


Figure 3.5: **Rat cultures show increased correlation as compared to rat cultures at the same age.** Six measures are considered and are normalized to whatever mean is higher amongst the two compared groups. *, ** indicate statistical significance of the difference between the groups at levels of confidence of 95% and 99%, respectively. Mouse statistics are based on $n=5$ cultures and rat statistics on $n=4$ cultures. Culture ages at the time of recording were selected so that both groups had the same mean age of 19.5 days *in vitro*.

related to the general excitability and not just to the synaptic development.

Finally, the spike sizes measure shows the mean of peak voltage in the recorded extracellular spike waveforms across all mouse and rat recordings (see section 2.5 for example waveforms). Surprisingly, we found a significant reduction in peak voltage for the recording from mouse preparations as compared to the rat preparations. This indicates that the two types of neurons are different in their excitability properties and that, in all likelihood, mouse neurons express a lower density of voltage dependent ion channels.

In summary, the comparison preformed confirmed that the mouse cultures are delayed in synaptic maturation as compared to rat cultures and thereby display reduced correlations at the same age *in vitro*. As far as these results can corroborate, our rat based preparations present all the features and developmental time course that have been described in literature and will therefore will be selected for the work carried out in the following chapters.

3.3 Evoked activity

An important feature of the MEA technology is the ability to induce generation of action potentials through injection of a current waveform into the extracellular electrodes. This is an important functionality as it provides means to provide input to the network and to control the culture activity. Past work have provided effective stimulation protocols and

showed that short current pulses can induce individual action potentials as well as a network response [16, 17]. This methodology was used to study response properties of single isolated neurons over long periods of time [18] and how several stimulation pulses interact with each other as a function of temporal proximity [19, 20, 21]. This approach was used to model sensory input by providing more complex spatio-temporal stimulation pattern and examining the extent to which the information present in the input signal can be decoded from the culture activity [22, 23]. Interestingly, it was shown that high frequency stimulation can break down the synchronized bursting structure of the culture activity, presumably in analogy to brain structures which exhibit higher frequency content when subjected to a high volume of input during active sensory processing [24].

To demonstrate that our system is able to effectively interface with the culture and provide input, we present data from a stimulation session where 120 test pulses were applied every 5 seconds (see section 2.5.2 for technical details). Data for two distinct stimulation sites is shown. Figure 3.6 A-B shows raster plots of the stimulation responses (at the different sites) averaged over all channels in a $500ms$ window after the stimulation pulse, as well as a cumulative PSTH. The PSTH is bimodal with a sharp peak observed within the first $25ms$ after stimulation and a second, significantly wider and less defined peak which lasts to typically lasts about $200ms$ after stimulation. The first peak is considered to represent direct responses, i.e., spikes elicited directly as a result of the stimulation pulse without synaptic mediation. The second peak is thought to be a manifestation of a multi-synaptic reverberating activity in response to the first step of activation. Indeed, it is evident from the response rasters that the first stage of response is significantly more repeatable than the second one which not always present. This is compatible with the above interpretation as direct responses are spikes generated due to a stimulation induced localized depolarization and depend only the specific biophysics and geometry of the neuron so they are expected to occur at a set delay and low jitter. The reverberating response, on the other hand, is a complex phenomena which depends on the network state preceding the stimulus so it stands to reason that it would show large variability or even fail to propagate on occasion. Nevertheless, it should be noted that even the direct responses were far from operating at a 100% success rate, a single neuron reproducibility issue that has been under much debate within neuroscience circles [25, 18].

Comparing between the responses to the two stimulation sites it is evident that they differed in direct responses with stimulations in channel 71 producing a second direct response peak which is also observable as a vertical line in the response rasters. The reverberating response did not show conspicuous differences in shape or latency although it seemed somewhat smaller. Another view on the differences between the two stimulation sites is given in figure 3.6 C-F which show spatially resolved response rasters and response maps for all participating channels, averaged over the stimulations. The spatial response profile appears to be very similar comparing the two stimulation electrodes - each channels showd s similar

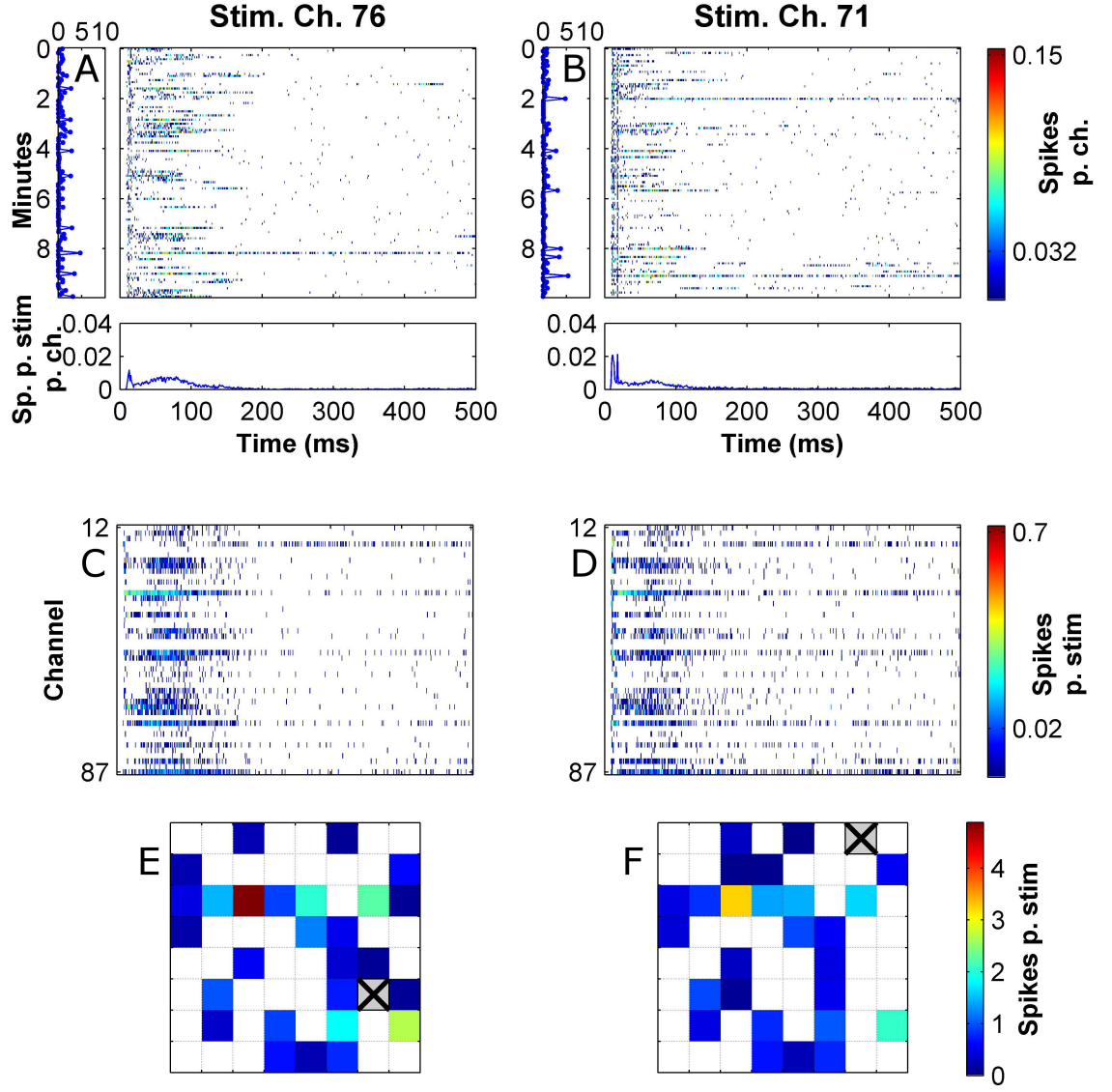


Figure 3.6: Stimulation pulses at different electrodes vary in direct responses but produce a similar reverberative responses. Test stimuli were applied every 5 seconds. (A-B) Main panel: Each line is a response raster for one test stimulus averaged over all channels. Left panel shows the sums of the responses shown in the main panel over the post stimulus observation time window (i.e., number of spikes per channel observed in 500 ms period post stimulation). Bottom panel shows the average of the response rasters over all stimuli. This is the PSTH. (C-D) Spatially resolved PSTHs, i.e., each line is a channel PSTH. (E-F) Stimulation response maps showing the sums of the PSTHs in (C-D) in the actual spatial locations. These response maps only show channels with a stimulation response that is significantly higher than background spontaneous activity for that channel (see section 2.5.2 for selection procedure). A,C,E and B,D,F show response data for two stimulation sessions applied to two different electrodes (indicated in E,F) run one after the other in concession on the same culture.

strength and duration of activation. There are some differences in latency but these were relatively unpronounced, at least to the naked eye. Although we did not study this in depth, it was our impression that different stimulation electrodes differ in mainly whether or not they are able to produce a reverberating response. However, once this response was elicited it seems to be stereotypical, i.e., each culture develops to take on a particular identity which is conjured whenever a synchronized burst occurs regardless of the site of induction or if it is spontaneous or evoked. It has been suggested that the lack of sensory input during culture development drives it into a degenerate state of over connectedness which might explain this rigidity. On the other hand, it should be noted that distinct yet overlapping responses to different stimulation sites have been reported [26]. Additionally, decoding of spatial stimulation information from culture data has been successfully demonstrated [27] so this system might nevertheless model genuine neural coding mechanisms from *in vivo*.

3.4 Plasticity induction in the presence of dopamine

Mature neuronal cultures abide to the principles of spike timing dependent plasticity (STDP), demonstrated in a paired pulse paradigm [2]. Modulation of the effective STDP window by dopamine has also been shown [3]. These results have raised the interesting possibility that neuronal cultures grown on multi electrode arrays could be used to study how plasticity operates at the network level. This sparked a substantial body of work to devise paradigms for induction and observation of plasticity using just the extra cellular network recordings and stimulations. Initial efforts have focused on brief tetanic stimulations inspired by the original experiments discovering LTP and which used this stimulation protocol [28]. Positive reports employing tetanus based induction have reported either a generalized potentiation in evoked responses which could be observed using simple measures such as summated response over all MEA electrodes [29, 30, 31] or more subtle effect that did not involve global change but rather antagonistic changes to the different channels and required more sophisticated multi-variate analyses to observe [32, 33, 34]. The later type of plasticity was observed both in evoked responses as well as in spontaneous activity. Indeed that tetanus induces a global potentiation is not surprising given that the original LTP experiments involved potentiation in the LFP measurements which represent large populations of neurons. However, it is known that neuronal systems employ homeostatic mechanisms to keep the general excitation levels constant [35] so such extreme modifications to activity are likely to be unphysiological. In that sense it is interesting that more subtle forms of plasticity are observed in the multi dimensional aspect of the activity. However, it is unclear why similar protocols produce such difference in outcome in different studies and different labs. Later work has shown that low frequency stimulation protocols can also induce changes in spontaneous activity of the subtle type [33, 36]. This result is interesting as natural input during real-life behavioural learning is probably more similar to such low frequency signals than to tetanus. Obviously, behaviour

in general and learning in particular are a closed loop process and this was modeled, to a certain extent, with feedback systems where the stimulation pattern was directly informed by the preceding neuronal activity [37, 38]. These important works showed that the direction and extent of plasticity can be controlled to follow bespoke criteria and therefore established that they are indeed relevant for goal directed learning.

As mentioned above, the quest to find plasticity in neuronal cultures grown in MEAs has produced successes but also contradictory, controversial and negative reports [26, 39]. Here we provide our own contribution to the discussion by applying one of the reported protocols to our mouse cultures and checking for plasticity. Additionally, as reviewed in section 1.2.1, neuromodulators have been shown to be strongly associated with neuronal plasticity and their presence or absence can strongly affect the direction of change (i.e., potentiation or depression) or even abolish it altogether. Moreover, neuromodulators have been shown to operate in both a tonic and phasic mode, where the phasic discharges are thought to act as a reward signal and whose timings are important for selecting neuronal activity that is relevant for the rewarded behaviour. Since neuromodulators have not been used in conjunction with plasticity and neuronal cultures on MEAs we decided to include a phase within our protocol where dopamine is introduced just for the induction phase and washed away afterwards. This to mimic a phasic mode of dopamine operation and to check if it enables the plasticity.

We elected to use a tetanus based protocol based on [29]. The reasons for selecting this protocol are as follows: Firstly, some of the past plasticity work on MEAs did not include a control to verify that the observed changes are due to the stimulated activity and not an artefact. Although this may seem unscientific it is a consequence of the nature of the system where each sample takes a long time to produce, maintain and measure. As a result, achieving a high n-number for both experiment and control is in some cases impractical. Our protocol works around this by exploiting the fact that neuronal cultures on MEAs can be used continuously for many recordings without compromise so we ran all experimental and control sessions on the same culture consecutively. Secondly, more complicated protocols such as the ones that apply stimulation in feedback from the recorded activity would require a sophisticated drug application system which is not currently available. This protocol includes a tetanus epoch of just a few minutes which offers a convenient time frame for manual addition and washing away of the drug.

Figure 3.7 shows a schematic of the experiment. The protocol catered for examination of both spontaneous activity and evoked responses. Each measurement epoch comprised a period of 10 minute recording spontaneous activity, followed by 4 x 10 minute periods of recording under 0.2 Hz test stimuli applied at 4 different electrodes, respectively. The electrode identities and amplitudes of test stimuli were selected to produce obvious evoked responses based on a pre-experiment examination. The measurement epochs were separated by 3 induction epoch running an 'associative tetanus' as proposed by [29]. 'Associative tetanus' is a stimulation paradigm designed to induce an association between two stimulated

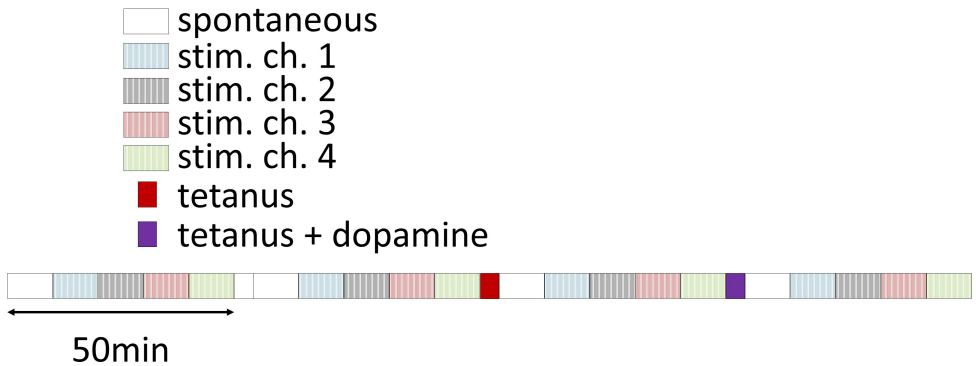


Figure 3.7: Outline of the combined dopamine and tetanus open bath plasticity experiments.

populations. The primary channel produces a tetanus pulse train consisting 50 pulse sets at 0.2Hz each consisting of 50 pulses at 20Hz . The secondary channel produces 50 single pulses at 0.2 Hz in phase with the tetanus pulse sets, i.e., each stimulation pulse in the secondary channel is timed to occur in the middle of a set in the primary channel. The primary and secondary channels were selected randomly out of the 4 stimulation channels used in the measurement epochs. The 3 induction epochs are as follows: (1) a sham (control) 'associative tetanus' executed by the signal generator with pulses of 0mV amplitude. (2) An actual 'associative tetanus' where the amplitudes for the primary and secondary channels are the same as those used in the test stimuli in the same channels during the measurement epochs. (3) An 'associative tetanus' as above where half of the culture media (0.5ml) was first removed for later use and $100\mu\text{M}$ dopamine•HCl was added. After the termination of the tetanus the dopamine containing media was replaced with the portion earlier removed and the final examination epoch was carried through. It should be noted that removal of half of the media during the 3rd induction epoch caused a slight but noticeable increase in the recording noise so the spike detection thresholds in the earlier measurement epochs were matched to the last one to avoid biasing of the results.

3.4.1 Examining changes in response to stimulation

Figure 3.8 shows example stimulation response data for the 4 measurement epochs in one of the tested cultures. Data is presented as explained in section 3.3. Baseline refers to the initial measurement epoch performed prior to any induction epoch. Control refers to the epoch taking place after the sham tetanus and the differences from the preceding epoch reflect spontaneous deviations in the culture activity. Tetanus and tetanus + dopamine are the epochs following the genuine induction phases. The differences between these experimental epochs and their immediate predecessors are compared to the difference between the control and baseline epochs so as to capture the effect of the induction. The baseline, control and tetanus epochs all show a similar PSTH profile and similar channel rasters. However, there

are also some noticeable differences. For example, the latency of the reverberating response seems to increase approximately half way through the control epoch, a change that is carried over to the tetanus epoch. Additionally, the reverberating phase of in the control PSTH is smaller than in the baseline and this is observed as reduced intensity in some of the channel rasters. These un-induced changes demonstrate the importance of employing such control epochs to assess how activity features change spontaneously.

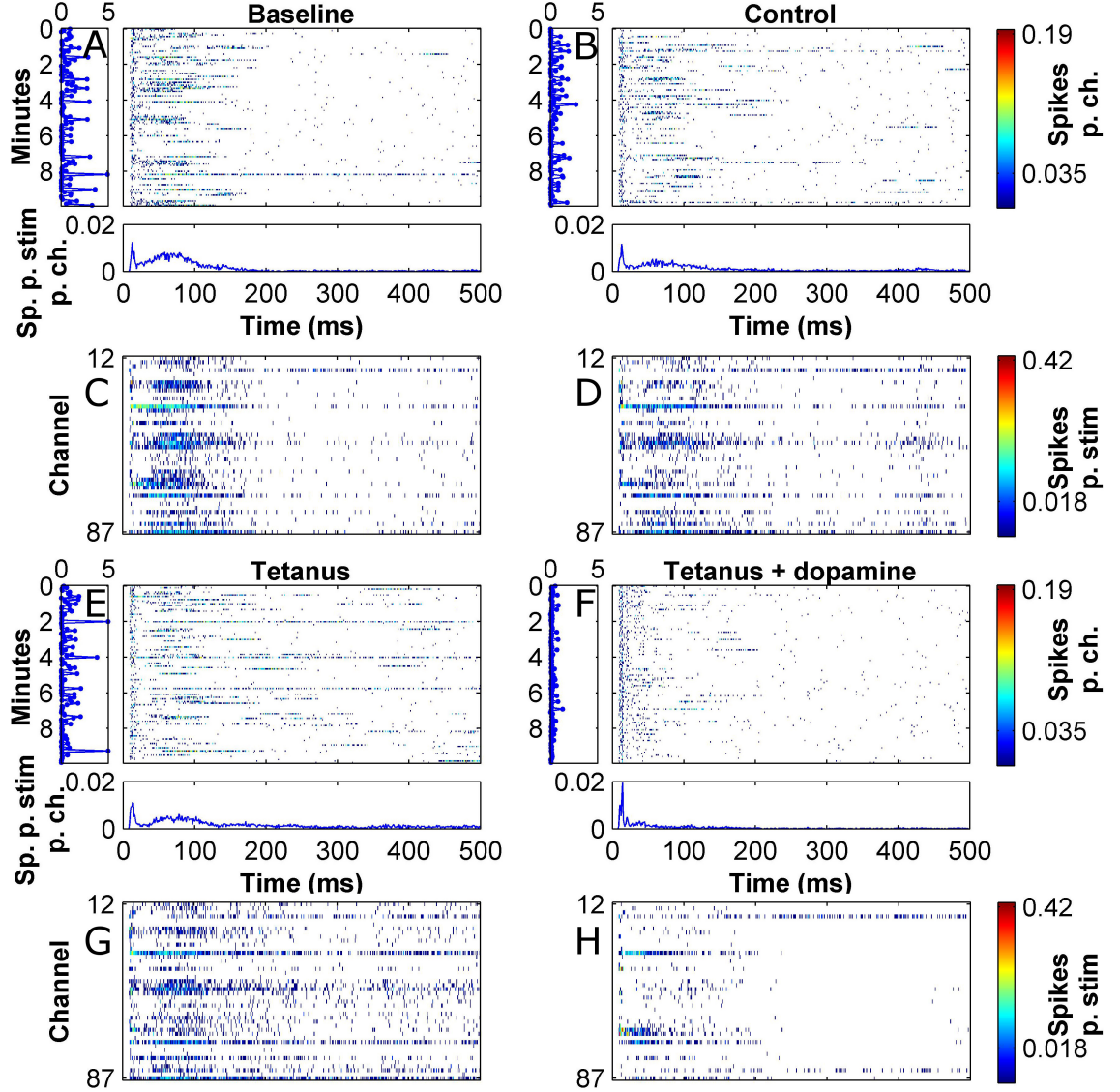


Figure 3.8: Tetanus combined with a dopamine pulse but not tetanus alone induces a depression of evoked responses. (A,B,E,F) Response rasters from the first stimulating electrode of each of the measurement epochs of the induction experiment. These are stimulation resolved (i.e., each line is a response to a single stimulation averaged over all the recording channels). (C,D,G,H) Channel-resolved response rasters of the same stimulation epochs. See caption of figure 3.6 for further details. Note an obvious decrease of evoked responses intensity following the tetanus induction in the presence of dopamine.

The tetanus + dopamine induction resulted in significantly more pronounced modifications to the evoked responses than the preceding inductions. The most obvious difference was the global reduction to the reverberating response in the PSTH. Most of the channels showed a marked decrease in intensity of responses although there were a few that actually increased. Another notable difference is that the direct response had become sharper. This global decrease in response is evident in the response maps in figure 3.9 where the number of responsive channels and their firing rate is markedly smaller after the tetanus + dopamine induction (recall that the response maps show only channels with significantly higher stimulation associated response in comparison with spontaneous activity).

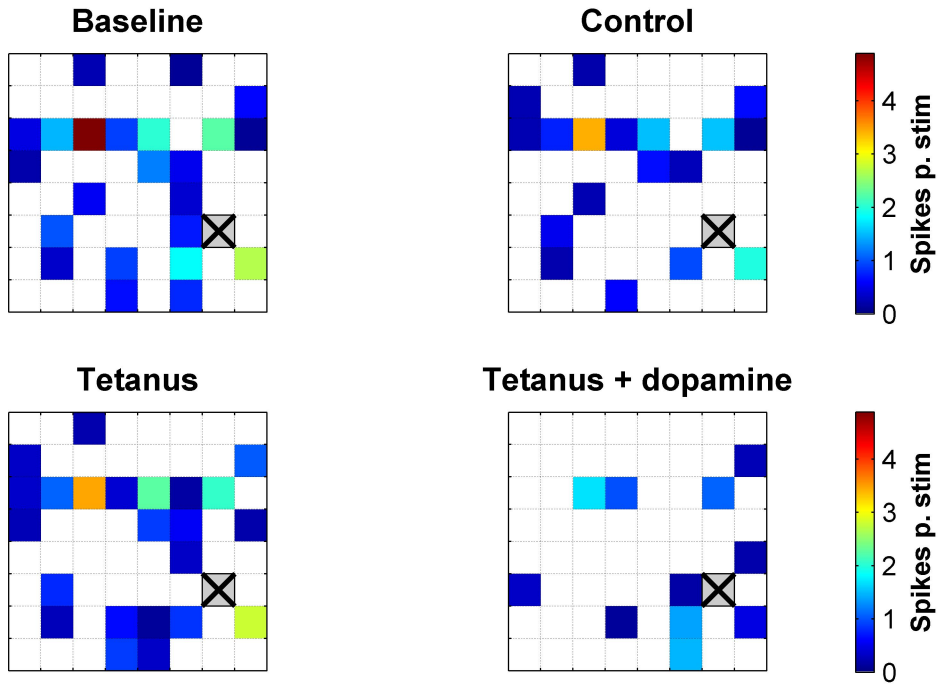


Figure 3.9: Tetanus combined with a dopamine pulse but not tetanus alone induces a reduction in the number of responsive channels. Stimulation response maps of the same data presented in figure 3.8.

Figure 3.10 shows a statistical analysis of the plasticity induction experiments which closely follows the one performed in [29]. In essence, channel responses for each stimulating electrode were compared in a scatter plot of pre induction vs. post induction responses and a linear fit was computed (figure 3.10 A-B). The slope for The 'associative tetanus' induction did not show a statistically significant difference from the one for the sham (control) induction (1.01 ± 0.07 vs. 1.07 ± 0.07 , 2-sided t-test, $p=0.5$). The slope for the induction performed under the presence of dopamine was significantly smaller, though (0.66 ± 0.09 , 2-sided t-test, $p=0.004$), indicating a general depression in evoked responses (i.e., across all channels). The potentiation index analysis provided results to the same effect. This analysis

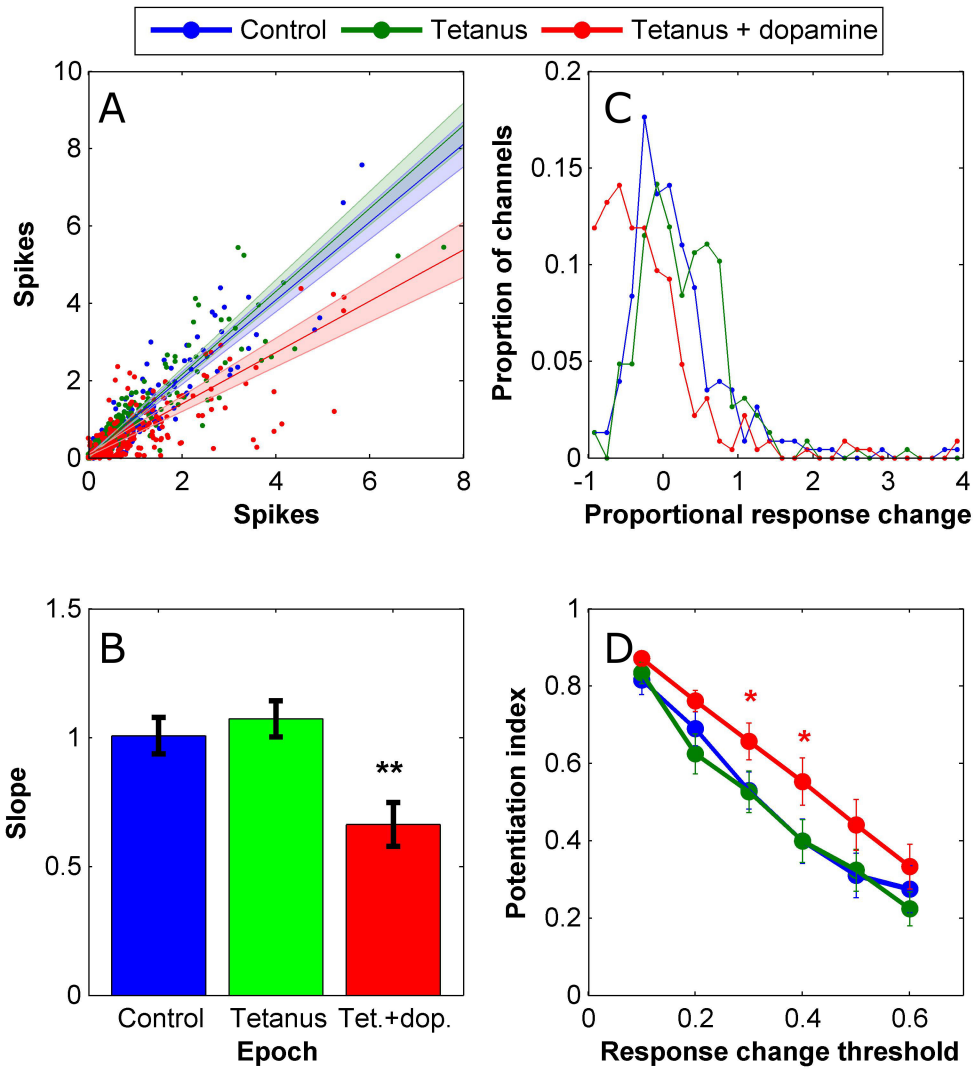


Figure 3.10: **Tetanus combined with a dopamine pulse but not tetanus alone induces a depression of evoked responses.** (A) Scatter plot of pre induction vs. post induction channel responses for the 3 induction steps of our protocol. Data from all tested cultures and from all stimulating electrode are lumped. The analysis, however, considers each of these groups to be an independent data set and fits a line to each. Plotted lines and shaded areas visualize the mean and SEM of these line slopes. Data is based on 4 cultures x 4 stimulating electrodes =(n=)16. (B) Comparison of fitted slopes from A. (C) Distributions of proportional changes induced in channel responses for the 3 induction steps of our protocol lumped as in A. For computation of potentiation index (PI) such distributions are generated for each data set. For each of these distributions the PI is the proportion of channels exceeding a threshold level of change. Finally, PI is computed for a range of thresholds and averaged over independent data sets (n=16 as in A). (D) Mean + SEM of potentiation index as a function of tested levels of change thresholds.

is based on generating distributions of proportional changes to the channel responses before and after the induction (figure 3.10 C). Potentiation index is a measure for comparing these distributions and is defined as the proportion of channels with absolute change exceeding a predefined threshold. By selecting the threshold correctly, a distinction between the distributions based on their width can be generated even if their mean is the same. In other words, this measure is designed to detect more subtle changes to the network activity that may include some of the channels experiencing large but antagonistic changes which cancel out when looking at the mean. In more common terms, one could say this is a variance or a second order measure. Since the appropriate threshold for making the distinction between the distributions is unknown, potentiation index is computed for several thresholds over the entire range of the data. It should be mentioned that the name 'potentiation index' is somewhat of a misnomer as it refers not to potentiation in the sense of strengthening but to absolute change. At any rate, applying this analysis to our plasticity induction data did not reveal any significant differences between the tetanus and control inductions. The tetanus induction in the presence of dopamine, on the other hand, showed a significantly higher potentiation using change thresholds of 0.3 and 0.4 (figure 3.10 D, 1-sided t-test, $p=0.034$ and 0.039, respectively). This, however, is not surprising given that a general depression was observed in the preceding slopes analysis.

3.4.2 Examining changes in functional connectivity

Since the afore-mentioned analyses did not reveal any tetanus-only induced plasticity we decided to try a yet finer probing of the network activity. This is based on the functional connectivity analysis which was reported to capture plasticity in response to tetanus [33]. Mathematical details and examples for computation of functional connectivity are given in section 2.5.5. In essence, the measure is based on locating peaks in the cross correlation function between channel pairs normalized to the number of spikes in the first channel. The size of the peak reflects the probability of recording a spike in the second channel following a spike in the first one at a time captured by the latency of the peak. This computation therefor results in 2 vectors, one holding peak sizes (also termed FC strengths) and the other peak latencies. Finally, differences in functional connectivity between recording epochs is measured as the Euclidian distance between the appropriate vector from the compared epochs. In our analysis we looked only at distances in the FC strengths vector because situations where the functional connectivity is lost completely (i.e., connection strength becomes 0) do not require special treatment. It has been claimed that this measure is more efficacious at detecting plasticity when computed over spontaneous activity [33] so we indeed used the spontaneous activity periods of recording in our protocol for its computation.

Figure 3.11 shows the changes to the functional connectivity over the different experimental protocols (measured as Euclidian distance from the baseline epoch) as well as the mean channel firing rate. The results show that the tetanus induction itself did not generate

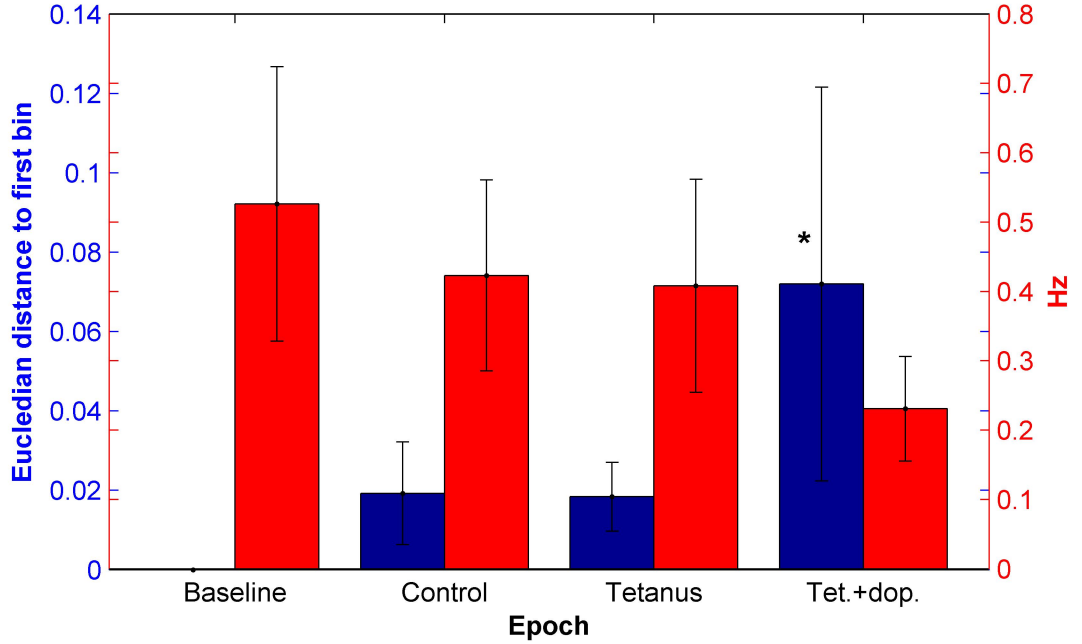


Figure 3.11: **Tetanus combined with a dopamine pulse but not tetanus alone induces a change to functional connectivity as well as a decrease to spontaneous activity.** Blue bars: Euclidean distance of the functional connectivity strength vector from baseline following each induction epoch. Functional connectivity was computed based on the spontaneous activity period in each of the measurement epochs. Functional connectivity computation requires a minimum number of spikes in each of the analyzed channel pairs to generate a meaningful cross correlation function estimation (see section 2.5.5) so only a subset of the possible recording channel pairs normally participate in the analysis. One of the cultures participating the the plasticity induction had to be removed as it had no channel pairs complying with the above criteria. Thus the shown data are based on n=3 cultures with 33, 10 and 179 computable functional connectivity pairs. Red bars: Mean channel firing rates in the same spontaneous activity measurement periods. This data are based on all n=4 participating cultures.

a change to the functional connectivity beyond naturally occurring fluctuations that were already observed after the control induction. A larger change was observed following the tetanus induction in the presence of dopamine which proved to be statistically significant (1-sided t-test, $p=0.026$). However, this change was also accompanied by a strong decrease in the mean channel firing rate which, for this data set, proved to be significant with only 90% confidence (1-sided t-test, $p=0.097$). In light of this change to the averaged culture activity, the observed shift in the functional connectivity measure should be taken with a grain of salt as it was designed to reflect subtle changes to the underlying culture structure in conditions where first order statistics (like mean firing rate) are stable.

3.5 Chapter conclusion

The main purpose of this chapter was to establish the standard neuronal culture on MEAs model system together with the accompanied Matlab analysis and show that the cultures are healthy and exhibit the diverse electrophysiological characteristics which have made them a successful neuroscience model system. Indeed distinct stages of development of network activity were clearly observed. These consisted of initial uncorrelated but widespread firing patterns corresponding to neuronal maturation followed by an increase in correlations and rate of synchronized events which indicate that the synapses are maturing. Further examination of the data revealed evidence for other neurobiological processes that have been described in culture. These included homeostasis of activity rates, existence of strongly intra-connected subnetworks and a gradual temporal narrowing of the synchronized events which has been attributed to a delayed maturation of the GABA neurotransmission system as compared to the glutamatergic one. These processes have not been studied here in depth but are taken as evidence that our cultures are healthy and in par with the literature gold standard.

Another important purpose for the work performed in this chapter is to examine the usability of mouse based cortical culture for MEA studies, as they have been seldom used in this context. We encountered difficulty in getting the mouse cultures to develop well on the MEAs and struggled with sub 50% success rates. In rat cultures, for a seeded culture to not develop well for several weeks was a rarity. Comparing electrophysiological parameters of the two preparations showed that the mouse cultures that did develop had a delayed synaptic maturation as compared to their rat counterparts, manifested in lower correlation values for same age *in vitro* and in synchronized events appearing later than expected from literature. Although the mouse cultures that did survive finally showed all the characteristics that could be expected from this type of preparation, their weakness in development and high failure rate led us to discontinue their use and switch to rat cultures for the following Ph.D chapters.

The final undertaking of this chapter was to explore a protocol for phasic application of dopamine using manual pipetting. We modified a common plasticity protocol to include a step where dopamine is ‘pulsed’ (through manual pipetting and subsequent washing) into the culture during the tetanus induction step. Without any dopamine, we were not able to induce a change in the culture activity, despite reports to the contrary in the paper from which the protocol was adapted. This should not come as a surprise as the literature is controversial in this regard and should just serve as a demonstration that further work is required for these system to serve as a useful model of plasticity. Following a tetanus induction which was performed in the presence of dopamine a significant depression was observed in the evoked responses which measured up to an hour following the induction. The spontaneous activity was also depressed but to a lesser extent. On one hand this could demonstrate and

enabling of LTD by the dopamine. The fact that this effect is present after the dopamine had been removed strengthens the possibility that this is a plasticity effect rather than a result of direct interaction of the cells with the agonist. Indeed a similar experiment had been performed in cortical slices and produced very similar results [40]. On the other hand, it is also known that in neuronal culture the mere action of media replacement drastically reduces activity (this will be made very clear by the results of chapter 5), an effect that could last several hours. Additionally, the presence of dopamine itself is known to have an inhibitory effect in the cortex regardless of plasticity [41, 42] and it is hard to rule out the option that a small concentration of the agonist is still present after the washing step and contributing to the observed effect. Under the constraints of the current bath application methods, it is impossible to run a dopamine pulse without these impinging effects. Indeed we could quantify them by using a set of control experiments but we cannot eliminate them.

To summarize, these dopamine pulsing results are promising in that they suggest a potential for dopamine to enable plastic behaviour in culture. However, this notion wasn't fully proven due to uncertainty about the effects of media replacement and of temporary interaction of dopamine with the neurons. This highlights the need for a precise solution exchange system whereby dopamine can be applied with high spatio-temporal precision and without change to other extracellular ingredients which could interfere with the activity. Such a system would allow interrogation into the fine temporal details of the phasic dopamine and volume transmission processes in general far beyond what was demonstrated in the above-described work. The following chapters in this Ph.D thesis will describe the development and establishment of a microfluidic based rapid solution exchange system where the drug delivery is rapid, precise and decoupled from other changes to the extracellular chemistry.

Chapter 4

Viability of neuronal cultures in microfluidic devices in static conditions and under flow

4.1 Introduction

As outlined in section 1.4 the purpose of this Ph.D work is to produce a model for phasic neuromodulator signalling by generating rapid agonist transients onto an entire neuronal culture. This is to be achieved using the interface shifting method in microfluidic devices. Applying this method involves using rapid flow rates at scales of 1mm/sec (the rational behind this figure is provided in section 4.2.1). Previous microfluidics work involving primary neurons used such rapid flow rates but just for short experiments lasting between minutes to 2 hours at most [43, 44, 45, 46]. Studies showing long term neuronal culture development under flow used much reduced flow rates where the convective forces were comparable to diffusion [47, 48, 49, 50]. Thus to avoid the complexity involved in getting neuronal cultures to survive long term under rapid flow we elected to follow an experimental paradigm whereby the cultures were initially grown in microfluidic devices in static conditions. After reaching maturity they were subjected to flow only for the duration of the experimental session. The first part of this chapter is dedicated to development of a protocol for long term culturing of primary rat neurons in microfluidic devices. As reviewed in section 1.3.2, this type of protocol is prevalent in the literature but the configuration of our devices, which were designed with the interface shifting method in mind, required specific adaptations.

An important part of the our experimental design is for the culture to be of restricted size (i.e., a microculture). This is necessary, firstly, because the interface shifting routine involves having a small proportion of the microfluidic channel area chronically exposed to the agonist, even between transients (see section 1.3.1). Thus to avoid such chronic drug

exposure, the culture needs to be located entirely outside the chronically exposed area. Secondly, it is important to note that an agonist pulse in interface shifting method actually takes the form of an agonist wave travelling along the long axis of the channel. This means that, depending on the flow rate and the geometry of the culture, cells at different locations along the channel may experience the drug at different times following the pulse command. In phasic neuromodulator signalling, the agonist molecules are secreted from nerve terminals that innervate the entire volume of the target tissue. Consequently, a neuromodulator pulse involves an approximately synchronized increase of agonist concentration over the entire innervated tissue followed by a decrease in concentration as the agonist molecules get locally re-uptaken [51]. It is important to note that, due to inhomogeneities in the spatial distribution of the innervating neuromodulatory fibers, different parts of the tissue still exhibit some delays in exposure to the agonist depending on their proximity to neuromodulatory synapse clusters. Nevertheless, these delays are small compared to the time scales of the global pulse [51, 52]. Because of the functional importance of timing in the neuromodulator signalling, it is essential that the microfluidic model does not exhibit increased delays in arrival of the agonist to different parts of the culture as compared to the *in vivo* tissue. To achieve the right timings, the flow speed and culture size need to be selected so that the drug traversal time across the culture matches the delays in the modeled tissue. The ability to control the culture size is crucial and the second part of this chapter will describe a method for generating microcultures which harbour small specific areas of the channel by utilizing microwells. The viability of these microcultures will be analyzed to establish their usability.

A final important topic that will be covered in this chapter is that of neuronal viability under rapid flow. Primary neurons are considered to be highly sensitive to shear stresses. Since this system is developed with long term plasticity in mind it is important to make sure that the culture is kept viable and functional for at least several hours under the applied shear stresses. It is also important to take into account that a functional neuronal tissue employs a large number of intrinsic volume transmission processes which comprise controlled secretion and uptake of active substances into the ECM (reviewed in section 1.2). These substances include neurotransmitters, hormones, neurotrophic and growth factors and are generally termed conditioning factors. Rapid flow is likely to interrupt with these processes by changing the concentrations of the conditioning factors or their spatial distributions. Since microfluidic flow has been scarcely used with primary neuronal cultures the flow rate limits have not been established and it is currently unclear what is the impact of each of the above-mentioned factors, shear stress and conditioning removal, on the culture viability. To characterize the effect of these factors we performed a viability assay under flow with a range of flow rates and media conditioning levels. In the tested range, we found a strong correlation between conditioning and viability but no shear effect. We established a protocol for media conditioning which, when used for flow, maintains the culture above the 90% viability mark for over 5 hours. Chapter 5 will further address the question of functionality and will describe

a characterization of the network activity under flow.

4.2 Long term neuronal cultures in microfluidic devices

4.2.1 Development of protocol

This section outlines the development of a protocol for long term culturing of primary hippocampal neurons in microfluidic devices. Long term culturing of cortical and hippocampal neurons has been established for over 30 years [53, 54, 55]. Recently, there has been an emerging use of microfluidic devices to culture neurons with increased control over the topology and to access specific neuronal compartments [56, 57, 58]. Nevertheless, neuronal cultures are infamous for their sensitivity to subtleties in the preparation technique and the materials that come in contact with the media or the cells and often require specific adaptations for the specific lab / application [59, 48]. These are discussed next.

Figure 4.1 shows the dimensions of the devices used in this study. The dimensions were selected so that, given the volumetric flow rates allowed by our flow system, a flow speed would be produced that is compatible with the desired agonist exposure times. Thus the main channel width was 1.5mm and the height was $65\mu\text{m}$ giving a cross section of $\approx 0.1\mu\text{m}^2$. Using a flow rate of 100nl/s gives an averaged flow speed of 1mm/s . Assuming that the long dimension of the culture would be less than a millimeter and that the culture would be positioned less than a millimeter from the agonist port then the agonist should reach the culture within a second and clear it a second later, which is the correct order of magnitude for neuromodulator phasic signalling [52]. Obviously this is just a back of the envelope calculation which does not take into account complexities in fluid dynamics and delays inherent to the flow switching system and its purpose is to provide a relevant geometry. A more rigorous examination of pulsing time scales will be performed in chapter 6 where the final microculture pulsing system is described.

The devices were bonded to glass cover slips using plasma bonding (see section 2.2 for details and more illustration of the assembled devices), oven sterilized, and then subjected to PLL surface treatment as detailed in section 2.3.

Due to the need to interface with a flow system, the microfluidic devices used in this work were made with biopsy punched ports of $\approx 0.8\text{mm}$ diameter which allow connection to the flow tubing by simple pressure fitting. This design contrasts with standard neuroscience oriented microfluidic devices where the ports are typically of 8mm diameter [56]. In these standard devices the seeding proceeds through pipetting of the cell solution into the ports and allowing the cells to flow through the channel (flow is enabled by controlling for a differential media height across the inlet and outlet ports). In the case of these standard devices, the ports function as de facto reservoirs by holding a significant volume of media ($400\mu\text{L}$ each) and therefore protect the device for dehydration and serve as a source of nutrients. Due to

the smaller port size in our devices, plating was performed by injecting the cells into the inlet port using a gel loading tip. The volume of injection was selected to be larger than the internal volume of the device so as to fully flood it with cells. The devices used here had an internal volume smaller than $1\mu L$ (figure 4.1) and the injection volume was $2\mu L$. After completion of the injection the cells were left suspended in the channel volume and were allowed to settle down in the incubator. The lack of flow following the cell injection made this protocol more consistent than the flow based seeding in standard devices. In those cases too strong of a flow ends up in having most of the cells flow through the device without settling and therefore in inconsistent seeding densities. On the other hand, a down side to our design is that due to their smaller diameter, the ports in our devices only hold about $2.5\mu L$ of media each and therefore cannot effectively fulfill the role of media reservoirs.

The following subsections will outline the major steps taken during the development of the protocol to circumvent the issues encountered along the way. The development of the protocol did not include an in depth scientific investigation to prove all the observed effects and interactions as doing so would have taken a long time and would have been counter productive with respect to the global project. The information is therefore not statistically complete and is presented in the form of examples which are meant to provide an intuitive and heuristic guide for scientists who would want to employ these techniques in the future.

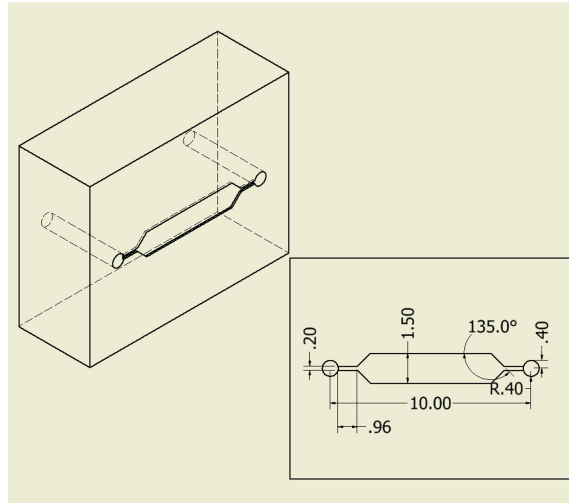


Figure 4.1: Schematics of the standard single layer microfluidic devices. All measurements listed in mm. Standard single layer microfluidic channels used in this section comprised both 2-port and 3-port (Y-shaped) configuration. Only the 2-port configuration is presented here for simplicity.

4.2.1.1 Evaporation and surface chemistry considerations

The initial incubation configuration explored was to apply a $200\mu L$ drop of media to the top of the PDMS surface to act as a media reservoir from which nutrients are exchanged and to preserve the aquatic environment. To minimize evaporation, the devices were further

kept in a closed petri dish next to a dish with 1mL DDW. The petri dish was kept in a humidified CO₂ incubator (Figure 4.2 A). The initial configuration also incorporated a 30 minute incubation with PLL solution as surface preparation. Cultures seeded in this configuration did not develop long term. The cells were initially healthy and adhered to the surface but the adhesion was non-uniform and by 5 days *in vitro* the cultures degenerated completely (figure 4.2 C-D). The main issue associated with this device configuration was that evaporation from the media on top of the devices was causing a rapid increase in the media osmolarity at a rate intolerable by the cells. We quantified this effect by measuring the osmolarity (Osmomat 030 by Gonotec) of the media on top 15 such devices after an overnight incubation. We found that the osmolarity drifted by $126 \pm 97 mOsm$ overnight, implying an evaporation rate of $49 \pm 20 \frac{\mu L}{day}$.

We tried to circumvent the evaporation issue by changing the drop on top of the devices every day (as opposed to twice weekly) and assessed the effectiveness by following the osmolarity of 4 devices for several days following the plating. Figure 4.2 B shows that the osmolarity in this case was stable but still very high (typical osmotic strength values for cell culture media is $\approx 300 mOsm$ and the osmolarity of our Neurobasal growth media is $225 mOsm$). A better solution was provided by switching to a maintenance routine where the devices were fully immersed in 2.5 – 3mL of culture media for the duration of the culture development (figure 4.3). Full details of this routine are provided in section 2.4. The volumes of media applied to each sample in this approach are comparable to what is used in standard cell culture samples so media could be changed just twice a week without incurring excessive osmotic drifts. After 3 weeks of culturing in this approach, media osmolarity never drifted more than $30 mOsm$. Beyond this, the initial patchiness in adhesion led us to suspect that 30 minutes of PLL incubation, which is adequate for standard open surfaces, might be insufficient in the case of microfluidic devices where the extreme surface to volume ratio might cause an increased flux of PLL molecules into the PDMS and reduce the effective concentration available for the glass surface. Consequently, we also modified the protocol to an overnight PLL incubation. With this modified protocol we were able to sustain neuronal cultures for long term (figure 4.4) but still not ideally, as will be described in the next section.

4.2.1.2 Considerations of factor circulation

Figure 4.4 A-B shows microscope images of two sides of an example device 12 days after seeding during which it was maintained using the modified protocol as described above. The part of the culture residing in the vicinity of the seeding port did not develop properly and was mostly degenerate. Remarkably, the part of the very same culture residing on the side opposite to the seeding port was able to develop properly and maintain a healthy appearance for several weeks. A hint as to the mechanism operating behind the above phenomena comes from devices where one of the ports was punched to be twice as big (figure 4.4 C-D). In this

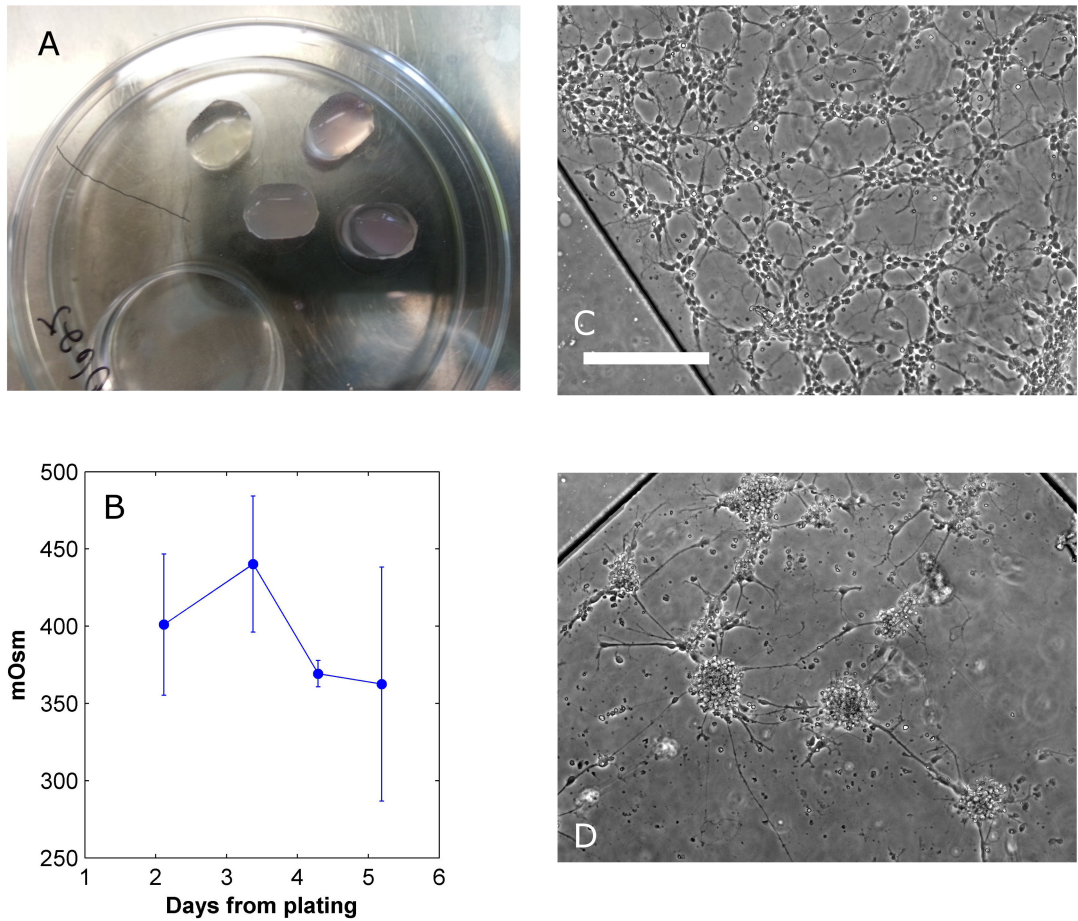


Figure 4.2: The ‘drop on top’ configuration results in excessive osmotic drifts and degeneration of the cultures. (A) Top view of a group of devices illustrating the ‘drop on top’ approach. (B) Osmolarity measurements taken from the drops on top of the devices in A during a maintenance protocol where the drop on top was changed every day. (C-D) Images of a culture growing in the ‘drop on top’ configuration and where the drop was changed only twice weekly. Images are at 2 and 5 days *in vitro*, respectively. Scale bar is $200\mu\text{m}$ long and is consistent for both images C and D.

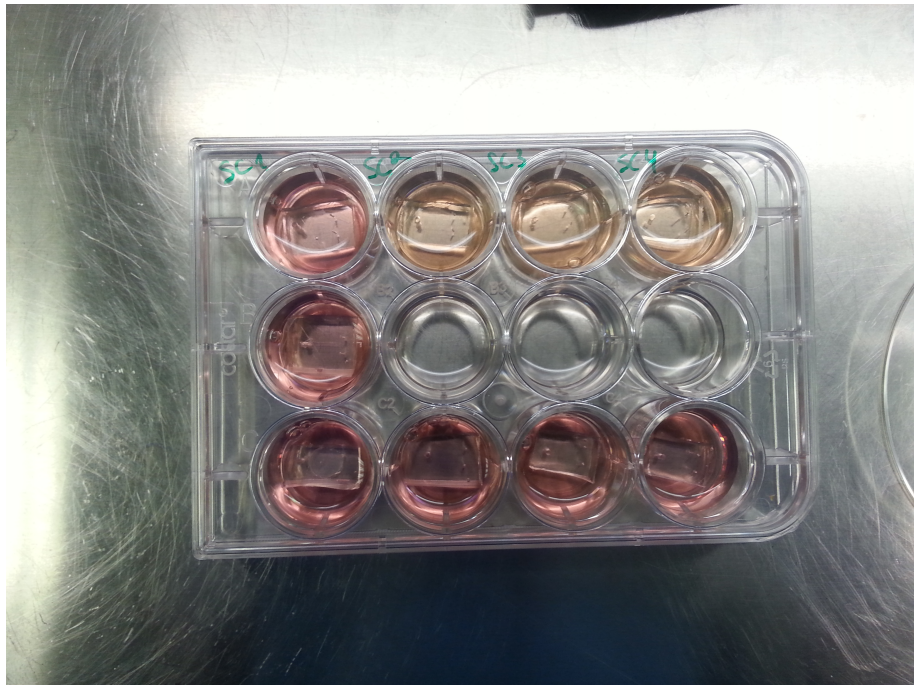


Figure 4.3: **The immersion configuration.** In this configuration, the devices were immersed in 12-wells with $2.5 - 3ml$ media each to prevent excessive osmotic drifts. This configuration required immersion 24 hours prior to seeding to release air trapped in the PDMS.

case the cells were seeded from one of the ports opposite to the large port. In these large port devices the whole culture developed healthily without any significant spatial differences. Another clue was provided by our exploration of devices with a larger architecture where the height of the channel was $1mm$ and its internal volume $\approx 20\mu L$. The density of the plating solution for these devices was calculated so that the plated area density would be as in the small devices, $2600 \frac{cells}{mm^2}$. Nevertheless, culture grown in these larger devices never exhibited any sign of such spatially arranged degeneration and typically developed well for several weeks (results not shown). We argued that the most likely explanation for the above observations is that the configuration of small devices and small ports does not provide adequate circulation to remove metabolic by-products and provide fresh nutrients to all parts of the culture. The fact that the degeneration occurred in proximity to the seeding port could be explained either by the port being blocked by lumps of cells or by a existence of a gradient of cell density along the channel. In both cases there would be a large unmet circulatory demand around the seeding port. In the case of the large port or the large devices, a stronger diffusive coupling between the culture and the external bulk media is enabled so in those cases circulation was not an issue. Since the configuration of small devices and small ports was required to properly interface with the flow tubing and to reach the required flow speeds we experimented with reduced plating densities in hope that these will have reduced circulatory demands. Indeed we found that by decreasing the plating density 6 fold (giving

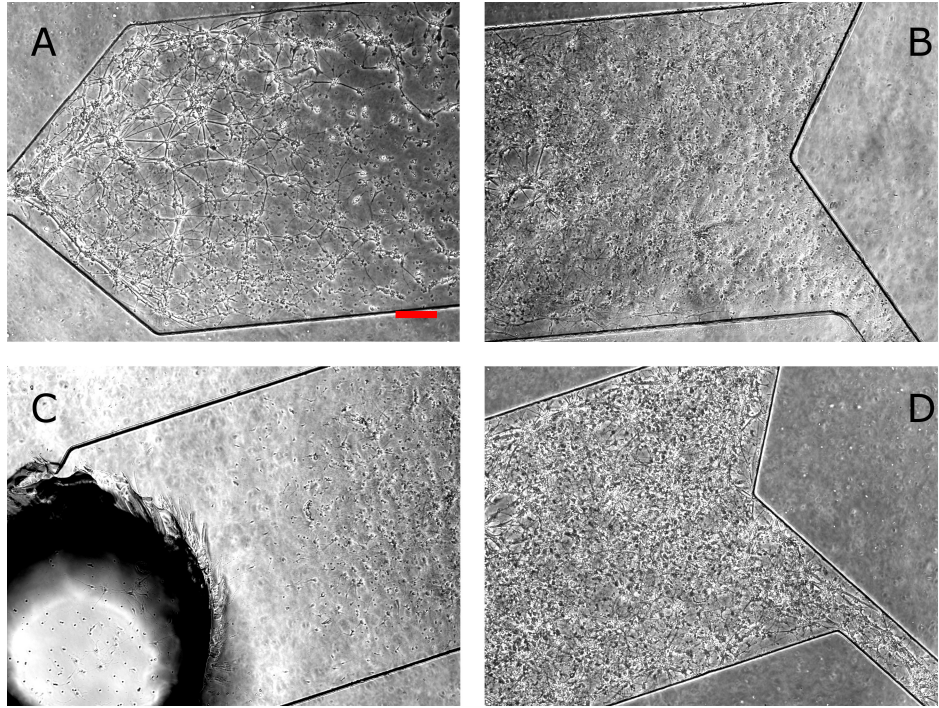


Figure 4.4: A circulation bottleneck can emerge in microfluidic devices. (A-B) Images of a culture growing in 3-port microfluidic devices where all the ports are 0.8mm in diameter. The images show the culture condition in the seeding port side and in the other side, respectively. (C-D) Images of a culture growing in 3-port microfluidic devices where one of the ports is twice as big (1.5mm). Images show culture condition in both sides of the device as before. Images were taken at 12 days *in vitro*. Seeding solution density was of $40 \times 10^6 \frac{\text{cells}}{\text{ml}}$ which is equivalent to $2600 \frac{\text{cells}}{\text{mm}^2}$ assuming homogenous distribution of the cells. Devices were maintained as described in section 2.4. Scale bar is $200\mu\text{m}$ long and is consistent across all images.

an area density of $\approx 450 \frac{\text{cells}}{\text{mm}^2}$) the spatially arranged degeneration phenomenon disappeared.

The observations described in this section demonstrate how microfluidic technology can impose conditions that are not normally met in standard preparations. The area density of $2600 \frac{\text{cell}}{\text{mm}^2}$ seeded in the earlier versions of the protocol is high but still commonly used for many applications involving neuronal culture. In those cases the culture is in immediate contact with a large volume of bulk media which readily supplies nutrients and removes by-products via diffusion. In our microfluidic devices, the internal volume of media is 3 orders of magnitude reduced ($\approx 1\mu\text{L}$) and it is only in this extreme configuration that circulation becomes an issue. This situation is similar to cases where non-vascularized 3D cultures develop a necrotic core due to the lack of oxygen and nutrient penetration.

4.2.1.3 Alternative bonding methods

Plasma bonding is a lengthy process that needs to be applied to each sample separately and therefore is not well suited for producing large quantities of devices. Additionally, it is not practical for more complex devices involving several layers as having to apply plasma bonding methodology to each layer separately makes the production of every single device very tedious. Consequently, we experimented with alternative bonding approaches that have been recently suggested for assembly of microfluidic devices [60, 61]. Complete protocols and illustrations are provided in section 2.2.

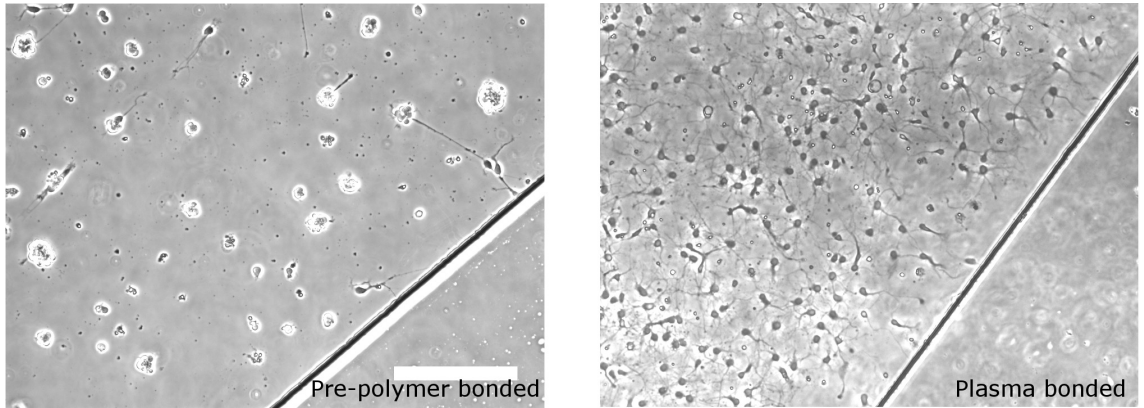


Figure 4.5: Contamination associated with pre-polymer bonding renders the surface unsuitable for neuronal adhesion. Images comparing a culture growing in pre-polymer bonded devices to one growing in plasma bonded devices. The images were taken at 5 days *in vitro*. Following bonding, the devices were subjected to identical surface preparation, seeding (density $7 \times 10^6 \frac{\text{cells}}{\text{ml}}$), and maintenance protocols (see sections 2.3 and 2.4). Scale bar is $200\mu\text{m}$ long and is consistent across both images.

The first approach attempted was to use the PDMS polymerization catalyst as an intermediate layer between the glass and PDMS bulk. The PDMS is dipped in catalyst solution, placed on top of the glass substrate and left to cure. This apparently induces further polymerization as well as partial covalent binding with the glass and results in a bond strength comparable or greater than plasma bonding [60]. We were able to achieve adequate bonding using this method but unfortunately the internal device surface proved to be completely inadequate for neuronal growth (figure 4.5. Interestingly, such a problem was not presented for other cell types such as astrocytes and HEK cells (data not shown)). This issue serves as another demonstration of the specific demands that are presented by neuronal culture. It is known that PDMS, when in contact with a surface, can contaminate the exposed areas around the point of contact through ‘leaching’ of PDMS oligomers or curing agent molecules. Indeed it has been shown that PDMS sometime acts as a source of contamination interfering with neuronal growth inside microfluidic devices [48]. The lack of adhesion reported here for the pre-polymer bound devices is probably an extreme manifestation of exactly these

contamination processes.

A different bonding alternative explored was that of using double sided silicone transfer tape [61]. In this case channel features are not engraved into the PDMS through soft-lithography but simply cut out of the tape which is consequently joined with the glass surface. A square PDMS bulk with punched ports is joined to the top side of the tape to complete the body of the device. Since this method does not disrupt the surface coating of the non taped parts of the glass and can be performed in a sterile hood it opens the door for a new surface treatment approach. With tape based assembly the device can be taped to a pre-treated glass (surface-then-bond) whereas previously, with plasma bonding, the surface coating chemicals had to be introduced and incubated in the assembled device (bond-then-surface). This shift in paradigm allows to utilize the device geometry to control which parts of the treated surface will be exposed and available for culture adhesion and therefore offers an easy way of controlling its shape and size. This concept will be critical for the establishment of the microculture geometry in chapter 6.

Figure 4.6 compares cultures grown in plasma bonded devices to ones grown in tape based and using the surface treatment paradigms appropriately as discussed above. The cultures are indistinguishable and appear to develop identically over the 12 days of inspection. This shows that the silicone tape is safe for use with neuronal culture and does not leach significant amount of toxins onto the surface or media. This tape based assembly approach will be cardinal for the multilayered devices described in chapters 5 and 6.

4.2.1.4 Extraction of PDMS

PDMS extraction is the last topic described with regards to the development of the basic protocol. As was apparent from the results of section 4.2.1.3, traces of curing agent or short oligomer chains can be harmful to neuronal cultures grown in the presence of PDMS. Indeed, even though the maintenance protocol achieved in section 4.2.1.2 did generally sustain neuronal cultures for at a couple of weeks *in vitro*, there were occasions where the cultures did not develop adequately. We reasoned that PDMS leaching might play a role in that inconsistency and therefore decided to try and employ a protocol for extraction of toxic species out of the cured devices. The protocol follows the suggestion from [48] and is detailed in section 2.1. Figure 4.7 compares cultures grown in standard devices to those grown in extracted devices from the same plating and using the same maintenance protocol. In this plating, the cultures in standard devices seemed to fasciculate early on and completely degenerated by 12 days *in vitro* ($n=5$). In the extracted devices ($n=10$) there was no sign of such degeneration. It should be noted that the extraction process involves immersing the devices in highly toxic solvents such as pentane and xylenes. When these are not properly oven-baked out of the devices a highly violent toxic effect is generated with the cells dying immediately upon seeding (figure 4.7 C). Faulty development in non-extracted devices was not always observed and could be attributed to a specific PDMS mixing batch or to interac-

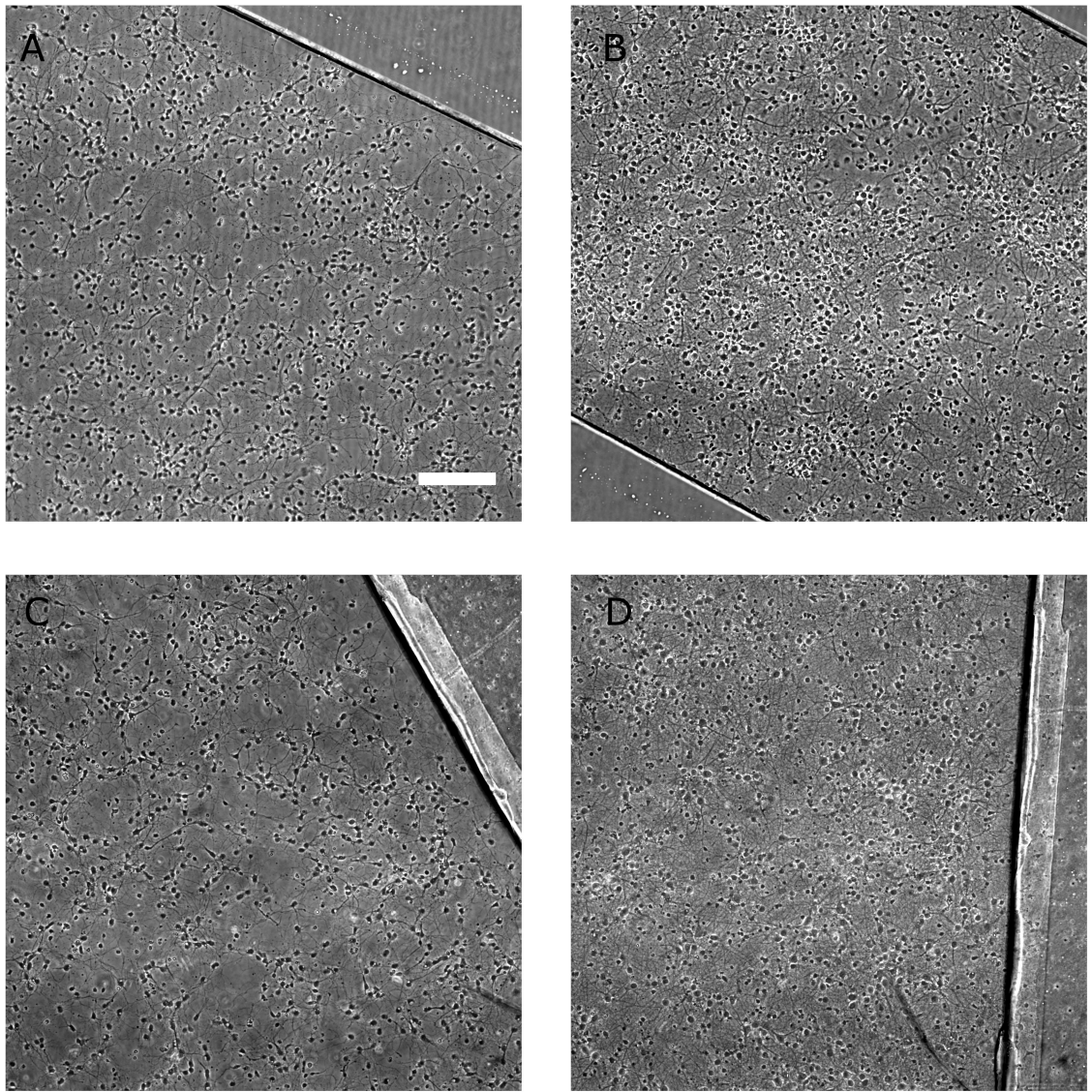


Figure 4.6: Tape based device architecture is fully compatible with neuronal culture. (A-B) Cultures growing in plasma bonded devices at ages 5 and 12 days *in vitro*, respectively. (C-D) Cultures growing in tape based devices at different stages of development as above. Plasma bonded devices were subjected to ‘bond-then-surface’ surface preparation approach whereas tape based devices were subjected to ‘surface-then-bond’ (see section 2.3). Both devices were seeded and maintained as described in section 2.4. Seeding density was $7 \times 10^6 \frac{\text{cells}}{\text{ml}}$. Scale bar is $200\mu\text{m}$ long and is consistent across all images.

tions with other factors. Nevertheless, to maximize the consistency of the preparations we added PDMS extraction to the standard protocol.

To summarize, we have developed a protocol for long term growth of neuronal culture in planar (1-layer) microfluidic devices. We reviewed what we consider to be the important factors in the development of such protocols, namely, osmolarity, circulation of nutrients and oxygen, ease of assembly and leaching of chemicals from the construction materials (usually

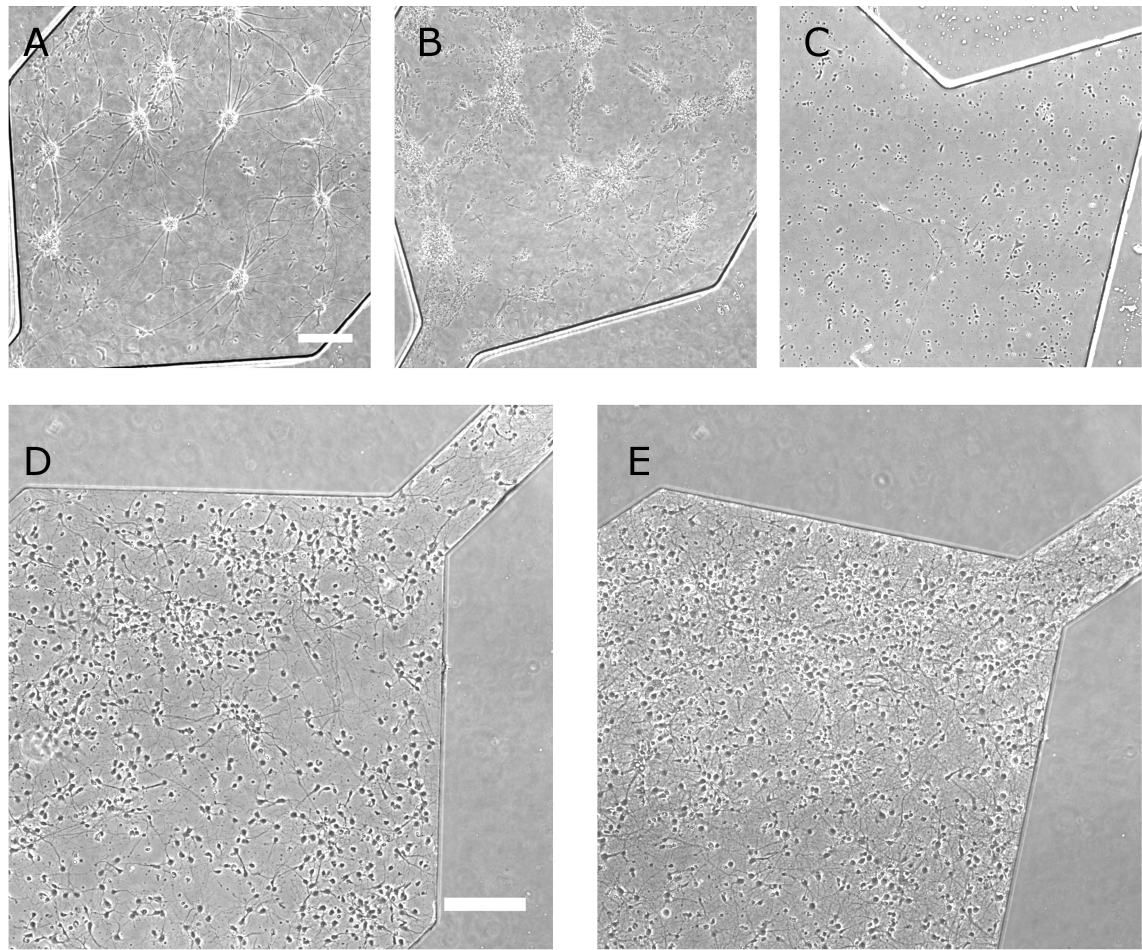


Figure 4.7: Non extracted PDMS devices can leach out chemicals that are harmful to neuronal growth. (A-B) Neuronal culture exhibiting adhesion and development issues that are thought to arise from PDMS leaching. Same culture is shown at ages 5 and 12 days *in vitro*, respectively. (C) Culture seeded in a device made from extracted PDMS which was not baked long enough for removal of noxious extraction chemicals. Image was taken at 2 days *in vitro*. (D-E) Cultures grown in extracted PDMS devices at 5 and 12 days *in vitro*, respectively. These images represent the typical cultures achieved for the final protocol incorporating all the principles discussed in this section. All devices were plasma bonded (section 2.1), subjected to ‘bond-then-surface’ surface preparation (section 2.3), seeded at a density of $7 \times 10^6 \frac{\text{cells}}{\text{ml}}$ and maintained according to section 2.4. Scale bar is $200\mu\text{m}$ long and is consistent across all images.

PDMS). Full details of the final protocol are provided in section 2.4. This protocol is the basis for all the subsequent device types used in this Ph.D thesis. All of them will use the same preparation and maintenance routines and will differ only in the seeding density and volume which require adaptation to the specific device and culture geometry.

4.2.2 Growing microcultures in plasma bonded devices

As explained in section 4.1, controlling the physical extent of the culture is necessary in order to apply the interface shifting method in a way that produces physiologically relevant concentration pulses. Here we describe confinement of the cultures into microwells of a desired size. To add microwells to our device geometry, we produced a PDMS sheet with rectangular holes via thin film spinning on a silicon/SU-8 mold comprising pillars in the shape of the required microwells (see section 2.1). To assemble the devices, the PDMS sheet was placed on a glass coverslip forming a reversible hydrophobic bond. The PDMS bulk with the engraved channel (as in figure 4.1) was then plasma bonded to the PDMS sheet while being manually aligned to position the microwell within the channel borders (figure 4.8). The devices were seeded at density of $20 \times 10^6 \frac{\text{cells}}{\text{ml}}$ and volume of $2\mu\text{L}$. The seeding filled the entire device volume with cells which settled arbitrarily on the exposed PDMS or inside the microwells. After the initial seeding the devices were inspected under the microscope to check if there is adequate inhabitation of the microwells and subjected to flushing and re-seeding as necessary. As shown in figure 2.1.2, an undesirable side effect of the way the PDMS sheet was manufactured is that the microwells are produced with an elevated ridge around them. The ridge caused a directing of the cells around the microwells rather than into them which was the main reason why flushing and re-seeding was necessary at times. After obtaining adequate microwell inhabitation, the devices were left in the incubator for 2-3 hours for initial adhesion of the cells, then media was pulled through with a 1ml syringe. This pulling had a differential effect on the cells depending on their location, i.e., most of the cells on the PDMS surface were ripped off and removed by the pulling whereas the cells in the wells tended to stay put as they were protected from the shear. In this way, isolated neuronal microcultures were generated and they were maintained as described in section 2.4.

Section 4.2.1.2 highlighted how, due to the small internal volume and narrow ports, our microfluidic devices can limit nutrient and oxygen circulation to the extent that necrosis is induced. In the case of the microcultures, however, the opposite extremity of factor circulation seemed to present itself. Initial attempts to grow microcultures under the the afore-mentioned maintenance protocol resulted in the cells showing an initially good adhesion but failing to show any subsequent development and degenerating altogether by 5 days *in vitro* (figure 4.9). This degeneration was similar in time scales to the one caused by the osmotic drift but seemed to be more aggressive as the cells did very little even in the direction of initial sprouting of neurites. This type of degeneration is known to occur in small / low density cultures even in standard preparations (i.e., open surfaces, not microfluidic devices) [59] where it is presumed that the neurons are not able to generate a sufficient concentration of conditioning factors around them to sustain their development. The typical solution in this situation is to grow the cultures in proximity to a large pure astrocyte culture which shares the same media and secretes the required conditioning factors. This auxiliary astrocyte culture is sometimes termed support culture. We followed this approach by adding two

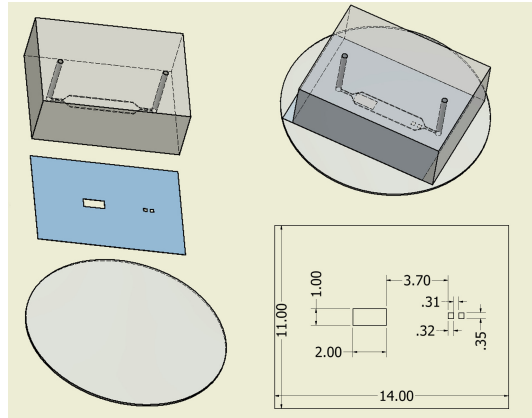


Figure 4.8: Schematics of the 2-layered microfluidic devices with microwells. The three components (PDMS bulk with an engraved microchannel, PDMS sheet and coverslip glass) of the device are shown separately and after bonding to illustrate how the the microwells are aligned to be within the channel boundaries. Dimensions of PDMS sheet are also presented in mm units. In this case, the microwells were of size $350 \times 320\mu\text{m}^2$. Dimensions of microchannel are as in figure 4.1.

levels of support culture. One was harboured in a large well situated within the device several millimeters away from the microcultures (see figure 4.8). A second one was a large culture plated outside the devices on the bare cover slip glass around the PDMS bulk. We found that the presence of these support cultures indeed prevented the afore-mentioned degeneration (figure 4.10) and that both of them together were required for best results (data note shown). We did not attempt growing pure astrocyte cultures for this as regular cortical cultures (which contain astrocytes) seemed sufficient to produce a beneficial effect.

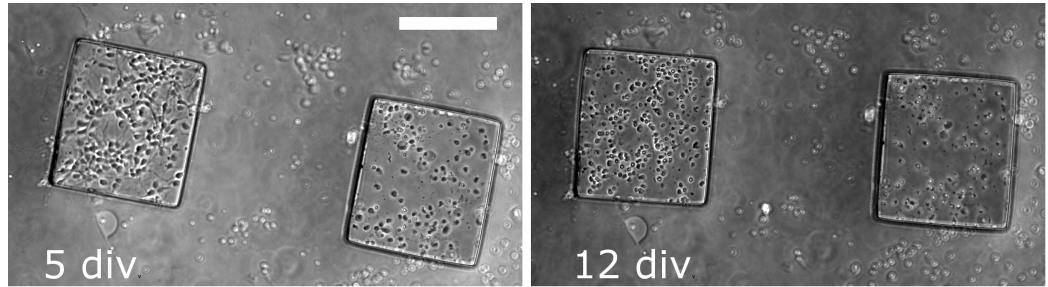


Figure 4.9: Neuronal microcultures do not develop without a support culture. Representative images of microcultures developing without seeding a support culture outside the device. The microwells were of size $300 \times 270\mu\text{m}^2$. Scale bar is $200\mu\text{m}$ long and is consistent across both images.

Since such microcultures are not a standard neuroscience model preparation in and it is unknown what is the smallest size they can be made while still developing properly, we decided to conduct a quantitative examination of their viability. To that end, we designed devices with 3 different microwell sizes and followed their development over 12 days *in*

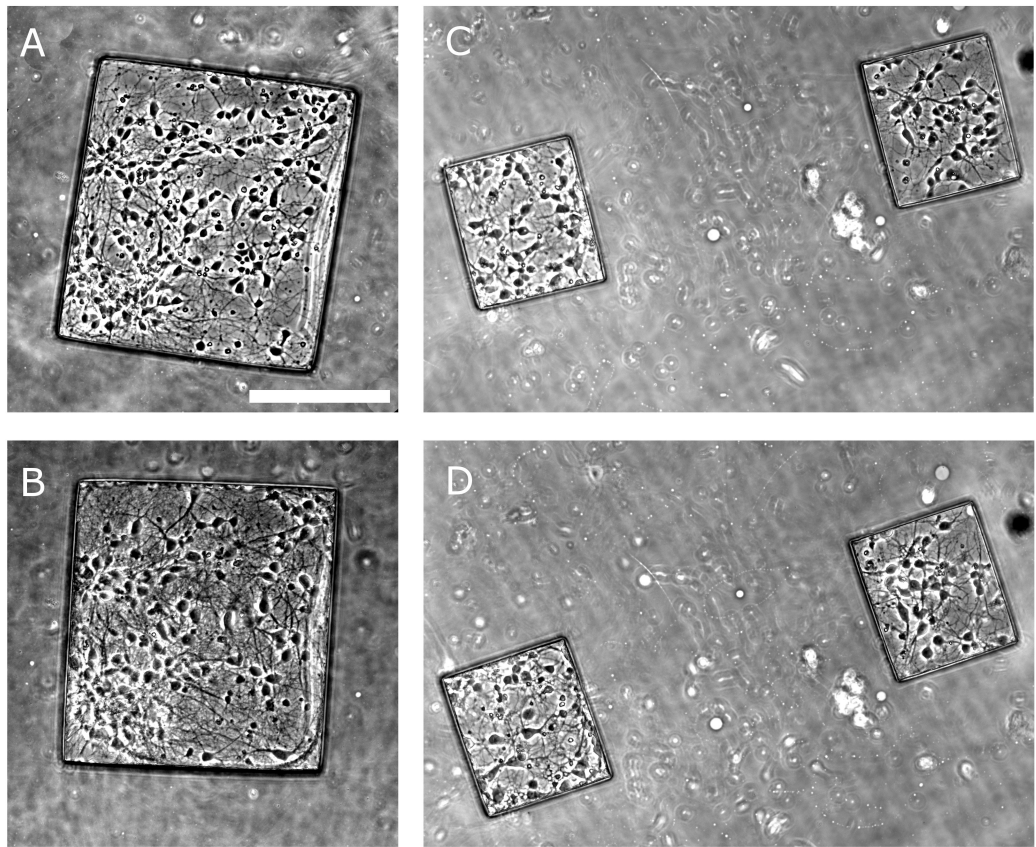


Figure 4.10: Development of neuronal microcultures. (A-B) Images of a neuronal microculture growing in a microwell of size $400 \times 370\mu m^2$ at 5 and 12 days *in vitro*. (C-D) Images of two neuronal microcultures at developmental stages as above in microwells of size $220 \times 190\mu m^2$. Microcultures were seeded at a density of $20 \times 10^6 \frac{cells}{ml}$, flushed and maintained as described in section 2.4. Scale bar is $200\mu m$ long and is consistent across all images.

in vitro. We counted the number of healthy cells in bright field images taken at 1, 5, 12 days *in vitro* and calculated the proportion of cells dying between consecutive counting time points. This data are presented in figure 4.11 as a function of the density of cells in the well at the preceding time point and grouped by well size. This is compared to the same statistic computed in the same way for images of the standard cultures from section 4.2.1 referred to here as macrocultures. It is evident from figure 4.11 A that, regardless of microwell size, the microculture death rates are strongly and negatively correlated with their density. This was corroborated with a linear regression analysis giving a statistically significant linear correlation (F-test, $p = 2 \times 10^{-4}$). The macrocultures did not show such a density associated death rate (F-test, $p = 0.26$) but the macroculture densities were much less variable so the analyzed density range was smaller. The averaged death rates of the macro- and microcultures are compared in figure 4.11 B. Microcultures of all 3 sizes exhibited a significantly higher death rate than the macrocultures (unbalanced t-test, $p =$

2×10^{-5} , 0.0012, 0.0027 for well edge sizes 200, 300, 400 μm , respectively).

Since microculture densities appeared to be a key factor in their long term viability we also performed a similar comparison with the microculture data restricted just to densities higher than $1500 \frac{\text{cells}}{\text{mm}^2}$. This density threshold was selected because the data beyond it did not show a density dependent trend which meant that the beneficial effects were saturated. Indeed the death rates at such high density microcultures were reduced and the large 400 μm ones exhibited death rates indistinguishable from those in macrocultures (unbalanced t-test, $p=0.23$). Smaller high density microcultures of sizes 200 and 300 μm still showed a significantly larger death rate (unbalanced t-test, $p=0.0012$ and 0.0012, respectively).

The above data are consistent with the notion that neuronal cultures need to generate an environment of conditioning factors around the cells to support their own development. Since this environment comprises secreted factors its buildup would strongly depend on the density and the size of the culture. Indeed the effect of both of these parameters is evident in the data shown here and a practical heuristic emerges that microcultures larger than $400 \times 400 \mu\text{m}^2$ and denser than $1500 \frac{\text{cell}}{\text{mm}^2}$ have a potential of developing as well as macrocultures.

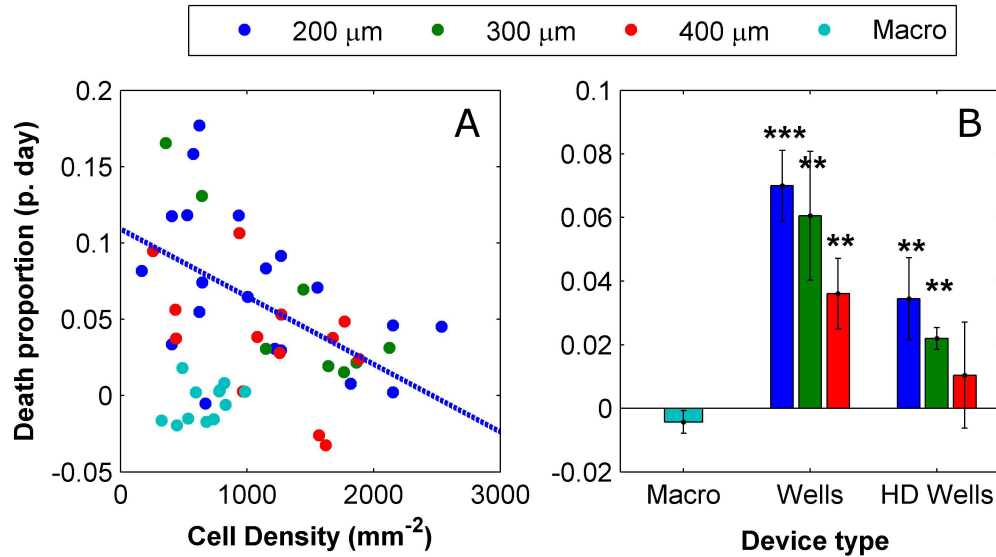


Figure 4.11: The viability of the microcultures is correlated with their density and size. (A) Scatter plot of the proportion of dead cells observed in the microcultures and macrocultures between consecutive counting time points as a function of microculture density. Each point represents a comparison between counts at 2 consecutive time points. Cells were counted at 1, 5 and 12 days *in vitro*. Death proportion is normalized to the number of days between the counts. Data is color coded according to microwell size or if it is a macroculture. (B) Comparison of mean proportional death rates between all the microcultures or microcultures with density higher than $1500 \frac{\text{cells}}{\text{mm}^2}$ and macrocultures. The data is based on 44 microcultures and 9 macrocultures from 4 different platings.

We would like to conclude this section by making a note about the quality of isolation of the microcultures. Since the devices considered here were assembled using plasma bonding, the surface treatment had to follow the ‘bind-then-surface’ approach. This means that the assembled devices were filled and incubated with surface coating solution (PLL) so all exposed internal surfaces were actually chemically prepared for cell adhesion. This means that cells from within the wells were free to send out neurites out onto the PDMS surface and even to migrate there. Additionally, the flushing procedure applied after the seeding was imperfect and sometimes left a substantial amount of cells on the PDMS sheet surface. This lack of restriction meant that after two weeks of growth the microcultures had significant innervation from neurons outside of the well (figure 4.12). Axons seemed to traverse the entire distance between the microwells and the large support well which was located 3.7mm away. This lack of isolation defeats the purpose for which the microwells were designed. This issue is solved in chapter 6 where tape based design allows a ‘surface-then-bond’ approach whereby only the well bottom is chemically prepared for cell adhesion.

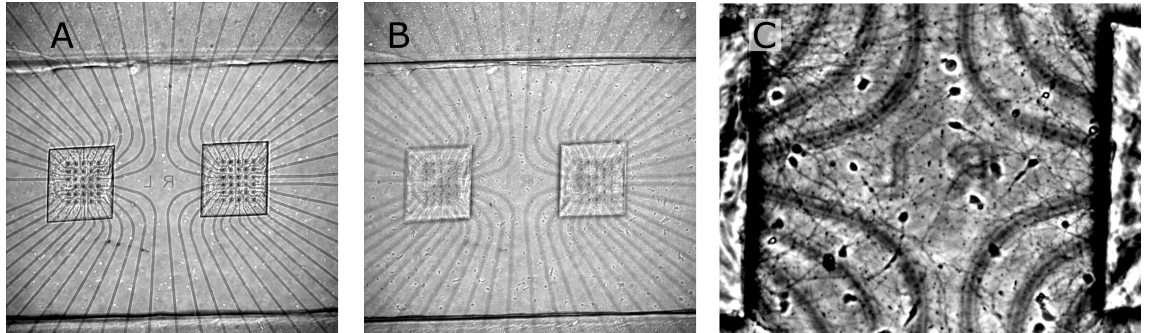


Figure 4.12: Microcultures are not well restricted to the microwell area. (A) Image of microcultures growing on top of commercial microelectrode arrays at 12 days *in vitro*. (B) Image of the same view field as in A focused on the top surface of the PDMS sheet. This image reveals the substantial inhabitation of the top surface by cells and neurites. (C) A zoom into the area between the microwells in B to highlight the presence of neurons and neurites outside the microwells. Microwells are of sizes $300 \times 270\mu\text{m}^2(L \times W)$ for scale reference.

4.3 Viability of neuronal cultures under steady microfluidic flow

4.3.1 Pilot flow study

The operation of the system in concern involves subjecting the neurons to flow rates in the order of millimeter per second. Thus, in this section as well as in chapter 5, we address the question of how well the cultures perform under flow. Primary neurons are considered to

be highly sensitive to shear stresses so we suspected that subjecting them to flow might be non-trivial and that there might be a limit to how high a flow rate they can bare. Since the interaction of primary neurons with flow is completely uncharted we conducted preliminary experiments where cultures at various ages were subjected to steady flow with growth media while being continuously monitored via time lapse imaging. The flow apparatus used for these experiments is described in section 2.8. These experiments seemed to develop in a stereotypical pattern: shortly after initiation of flow, the cells started losing the surface adhesion which was manifested by obvious fasciculation. In younger cultures where not too much ECM tissue had been built it could be observed that the fasciculation was accompanied by a retraction of processes (figure 4.13). By 20 hours, most of the cells appeared to degenerate. In older cultures rich in ECM this degeneration also involved complete detachment of the tissue, which was left floating inside the device volume.

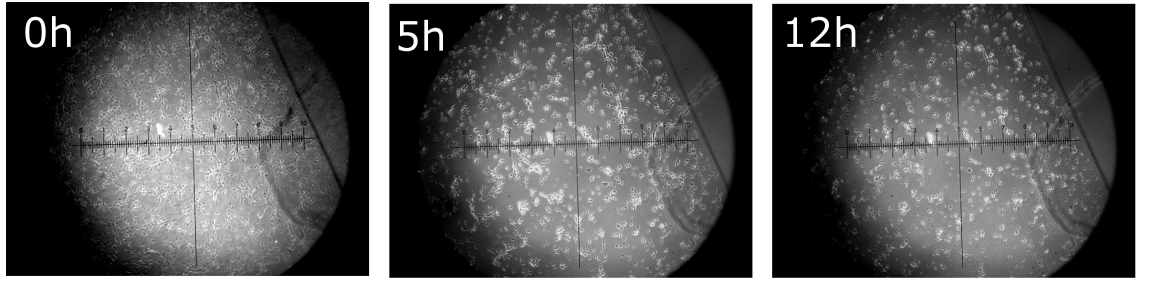


Figure 4.13: Neuronal cultures exposed to steady flow lose their surface adhesion, retract their processes and degenerate after several hours. Time lapse of a neuronal culture grown in the standard 1-layer microfluidic devices (section 4.2.1) placed under flow at 1 day *in vitro*. The flow rate was $1 \frac{nl}{s}$. Scale units: $\approx 100\mu m$

Initial experiments were conducted with the devices placed openly in the ambient environment while only plugged into a custom made heater system where heating resistors were brought into contact with the glass and the PDMS bulk and were controlled to $37^\circ C$ [62]. However, we had concerns as to how well this system controls the internal device temperature given that media at room temperature is pumped in. Additionally, maintenance of media CO₂ levels was based on connecting the pressure control system to a 5% CO₂ / 95% air gas supply. This configuration assured that the media in the flow reservoirs were fully CO₂ saturated but there was still a concern that as it travels through the tubes in the ambient air some CO₂ content could escape. To alleviate these issue, we built a custom made compact environmental chamber whose internal environment was controlled to $37^\circ C$ and 5% CO₂ (figure 2.8.1). The flow tubes were introduced into the environmental chamber through a small side hole before connecting to the devices. The tube configuration was purposefully selected such that the total tubing volume outside the environmental chamber was 3 times less than that of the internal tubing ($\approx 16\mu L$ vs. $\approx 60\mu L$). This meant that, while travelling from the reservoir to the device, the media spent triple the time inside the

chamber environment than in the ambient one so any CO₂ lost outside would necessarily have been reabsorbed. We also calculated that the residence time inside the chamber is at least 10 minutes which is more than enough to heat the media to 37°C given the micrometer scale of the tubing (this was verified with an inline flow thermocouple, PH-01, Multi Channel Systems). Nevertheless, the employment of the chamber did little to change the outcome of the flow experiments leading us to conclude that the basic physiological parameters of temperature and media CO₂ saturation did not play a major role in the degeneration.

Since conditioning factors are known to exert a protective effect on neuronal culture [59, 63] we explored the option of using conditioned media, i.e., media taken from a different culture for flow. We found that this had a pronounced effect on the cultures' tolerance in the sense that there was an initial flow period where the cultures' appearance did not seem to change. Additionally, even though fasciculation and degeneration still occurred, they developed much later, typically more than 10 hours into the flow session. Another interesting observation was that the rapid degeneration observed with fresh media flow seemed to occur regardless of the flow rate and presented itself even when the tubes were connected but the flow was set to 0 $\frac{nl}{s}$. These observations suggested that, when using conditioned media, a time window could be present where the culture is functional and useful experiments may be performed. They were also surprising in that the flow rate, i.e., shear, appeared to play a smaller than expected role in the adverse effects of flow. We therefore decided to conduct a systematic study to quantitatively asses the effect of conditioning and shear on the viability under flow and to establish what is the practical experimentation time window. Description of this study follows.

4.3.2 Quantitative viability analysis

Analyzing how media conditioning affects viability under flow requires an analytic measure of conditioning. Since conditioning involves a continuous secretion of factors into the bulk media, it seemed plausible that, a conditioning measure would be proportional to the length of time which the media was in contact with the cells. We produced conditioned by growing cortical rat cultures of prescribed densities in T-25 flasks with prescribed media volumes and without changing of the media. The precise protocol and the conditioning scale are provided in section 2.7. Roughly, every 3.5 days of incubation in the flasks *in vitro* are equivalent to 1 conditioning units.

We ran a large set of steady flow experiments on macrocultures growing in standard 1-layer devices. The experiments were conducted in a range of conditioning levels and flow rates. To provide a quantitative measure of viability these flow experiments also included a propidium iodide assay (protocol and example in section 2.8). In brief, propidium iodide was added to the flow medium so it was present around the cells for the length of the experiment. Intact plasma membranes of healthy cells are impermeable to fluorescent DNA-binding molecule. However, when cells die their nuclear material becomes exposed and

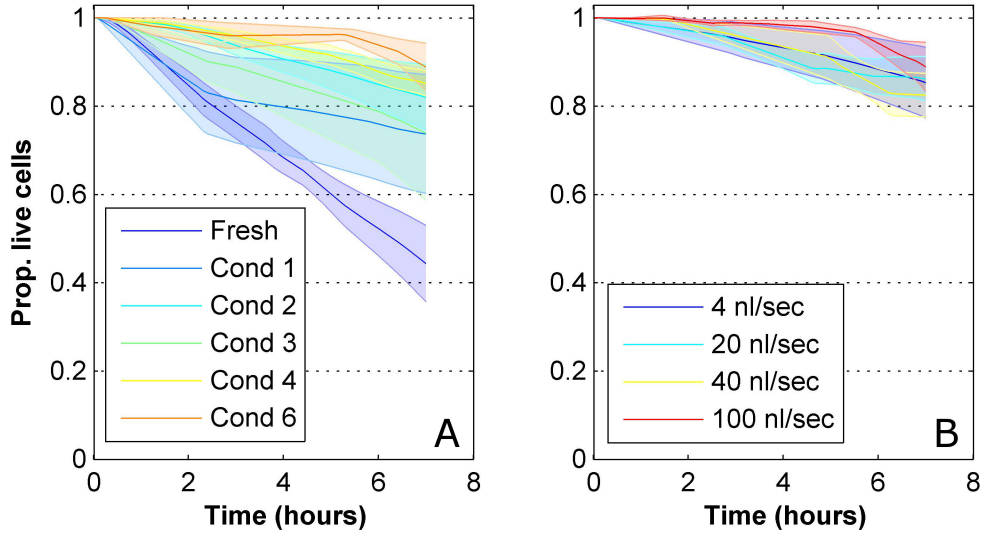


Figure 4.14: Using conditioned media for flow can significantly prolong the culture viability regardless of the flow rate. (A) Averaged viability curves for flow with media of increasing conditioning levels. Every curve averages data from several flow experiments where a propidium iodide assay was used to quantitatively assess the number of dead cells over time (full description is given in full in section 2.8). Example for such individual flow curves can be seen figure 4.15. The flow rate for all experiments was $40 \frac{nl}{s}$. Shaded areas depict the SEM. (B) Averaged viability curves as in A but where the flow rates are varied whereas the conditioning level is fixed at 4. The data is based on 36 experiments from 9 platings. Every curve except for Cond 6 in panel A is the average of at least 3 experiments from 2 different platings. Cond 6 is based on 2 experiments from one plating.

readily serve as a seed for propidium aggregation and therefore appears as a dot in fluorescent microscopy. These dots are counted to provide a quantitative measure of how many cells have died since the initiation of the flow. During a flow experiment fluorescent images were taken every 1-2 hours to generate a curve of the deterioration in viability. Figure 4.14 shows averaged viability curves for a range of conditioning levels where the flow rate is fixed and for a range of flow rates where the conditioning level is fixed. The observations made in the previous section are clearly manifested in these curves: increasing of the conditioning levels is negatively correlated with the death rates whereas increase in flow rates within the tested range is not.

To facilitate the statistical analysis we grouped the conditioning scale into 3 groups: Fresh media (same as before), intermediately conditioned (grouping conditioning levels 1 and 2) and highly conditioned (grouping levels 3-6). Figure 4.15 shows the averaged viability curves generated with new grouping as well as a control curve made without connecting the cultures to the flow system at all (static). The figure also shows a breakdown of the averaged curves into the constituent individual ones per experiment. Since the individual curves did not

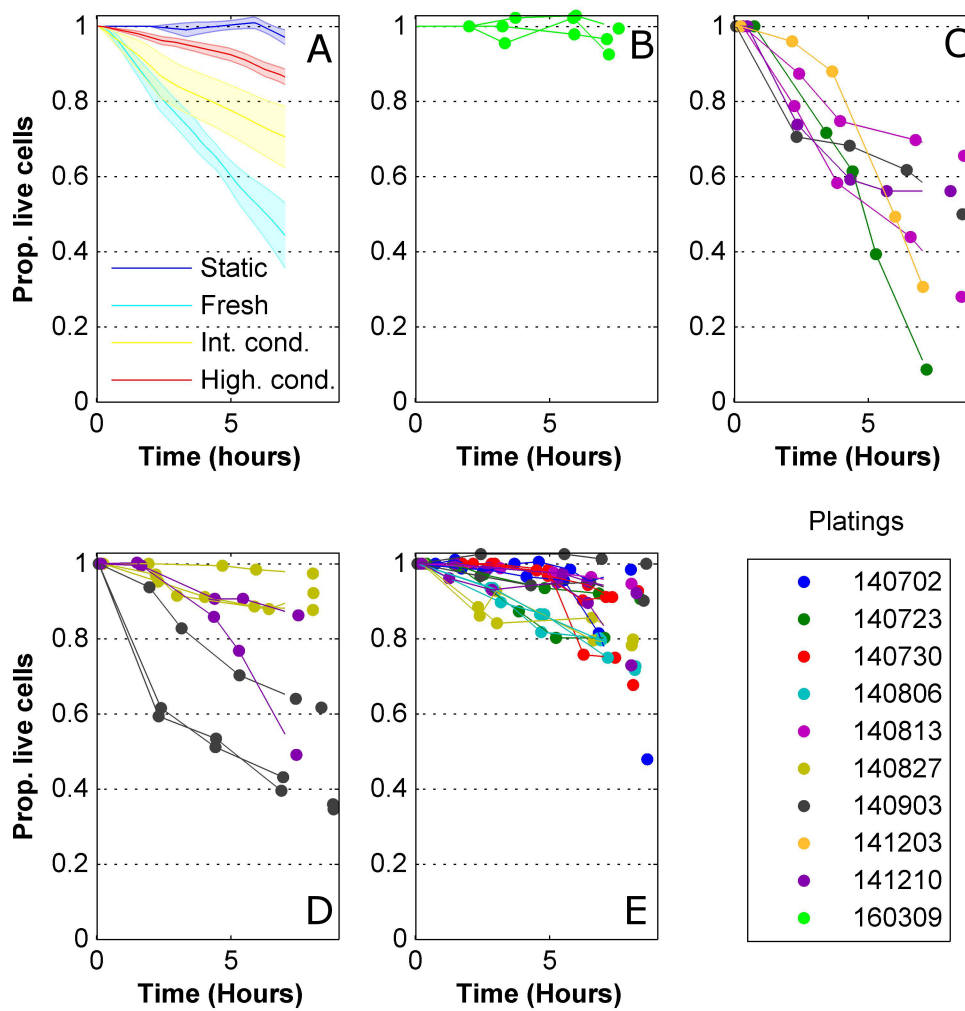


Figure 4.15: Individual viability curves do not exhibit any common temporal features so their average is linear. (A) Averaged viability curves for increasing conditioning levels as in figure 4.14 A but with a grouping applied to get improved separation (grouping specified in the text). The flow rate for all experiments was $40 \frac{nl}{s}$. An additional control curve is included where the devices were not connected to the flow system. (B-E) Individual viability curves from the experiments that were averaged in A. Each dot represents a fluorescent image where the number of dead cells were counted. The order of the panels B-E matches the order of the averaged curves as listed in the legend of panel A. Individual curves are color coded according to the date of plating of the given culture.

exhibit any conspicuous common time dependent features and as the averaged curves were strikingly linear we reasoned that a fixed death rate model (linear) would be a plausible a description of this data. In accordance with this notion, the statistical analysis was based on fitting a line to the viability time series of each experiment with a forced intercept at

(time=0, viability=1). The statistical testing was then performed on the fitted slopes and is discussed next.

Figure 4.16 shows a comparison of the fitted death rate slopes for various flow conditions. The conditioning levels of the flow media were shown to have a significant effect on the death rate (Figure 4.16 A, 1-way ANOVA, $p = 1.5 \times 10^{-5}$). However, flow under all conditioning levels still resulted in death rates significantly higher than control (unbalanced t-tests, $p = 2.1 \times 10^{-4}$, 0.049 and 0.021 for fresh media, intermediately conditioned and highly conditioned respectively). Thus we were not able to find a conditioning regime where the cultures were viable for long term under flow. To get an idea as to how much using conditioned media can extend the experimentation time, we calculated how long at least 90% of the cells will be alive, given the established death rates. This provided times of 1.3, 2.5 and 5.6 hours respectively for the 3 conditioning levels at hand. Given that highly conditioned media was used, changing the flow rate did not produce a significant difference (Figure 4.16 B, 1-way ANOVA, $p = 0.91$). The main experiments above were preformed with PEEK tubing. We also tested if changing the tubing material would affect the viability under flow. We found that stainless steel tubing gave the same results as the PEEK for flow with highly conditioned media. PTFE tubing, however, was surprisingly associated with a significantly higher rate of degeneration (Figure 4.16 C, unbalanced t-tests, $p = 0.95$ and 7.5×10^{-11} for stainless steel and PTFE tubing, respectively). Thus, The beneficial effect of conditioning seems to be absent when using PTFE. This could suggest that our PTFE tubing absorbs valuable conditioning factors or that it introduces contaminants into the media during flow. We did not further interrogate this non-trivial effect but it is important to make a note of how the tubing selection can affect these types of experiments. Finally, since all the conditioned media in this study was used straight from the culture flask we wanted to check whether it could be stored for later use as that would greatly simplify the experimental design. Consequentially, we extracted highly conditioned media, kept it frozen at -80°C for several weeks and then heated it back up to 37°C prior to using it for flow. We found that the frozen media did not preserve the beneficial effects of the conditioning and resulted in significantly faster death rates as compared to the media used directly from the flasks (4.16 D, unbalanced t-test, $p = 0.0073$). Interestingly, the performance of the frozen media was statistically the same as that of the intermediately conditioned media (unbalanced t-test, $p = 0.59$) so the benefits of conditioning were still partially present. It is likely that some of the conditioning factors degrade over time and are sensitive to freezing and thawing (e.g., large protein molecules) hence the above results.

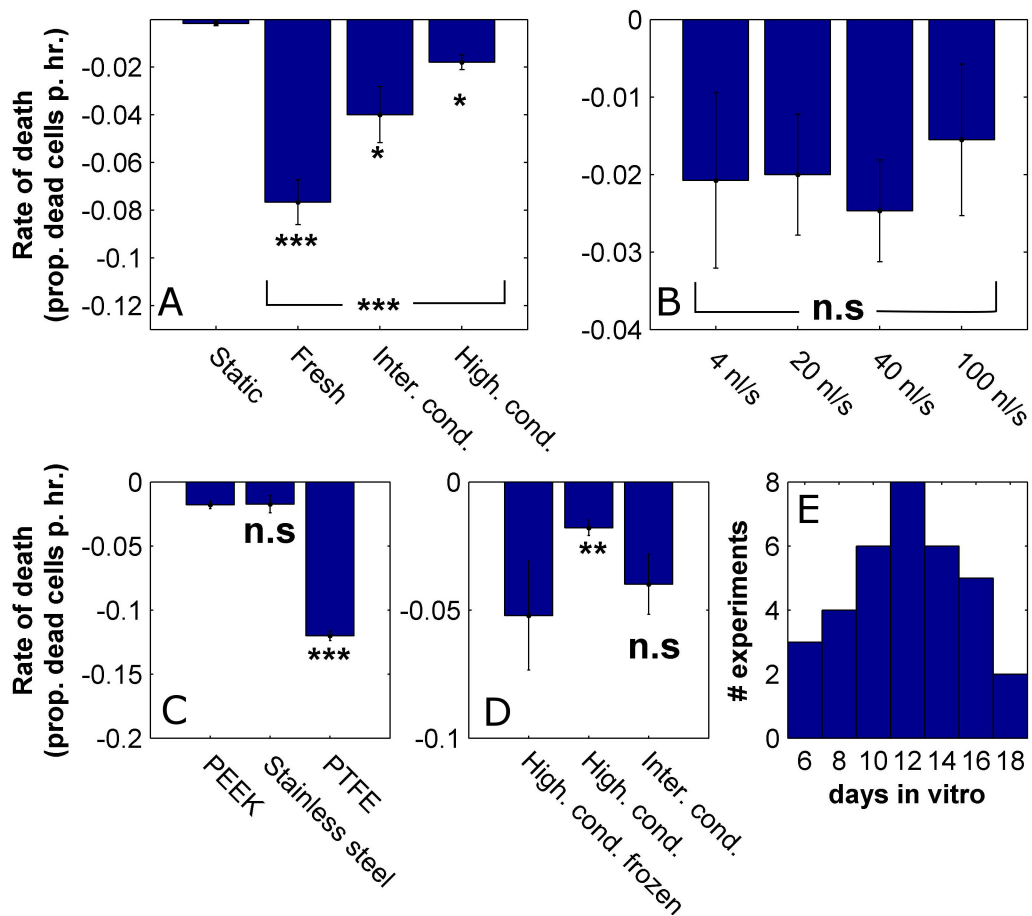


Figure 4.16: Death rates under steady flow depend on media conditioning levels and on the type of flow tubes but not on flow rates in the tested range. (A) Comparison between the measured death rates under steady flow for increasing media conditioning levels and for control devices. Experiments were identical in all other parameters (flow rate $40 \frac{nl}{s}$ and PEEK tubing). **(B)** Comparison between the measured death rates under steady flow for increasing flow rates (all highly conditioned media, PEEK). **(C)** Comparison between the measured death rates under steady flow for different tube types (all highly conditioned media, $40 \frac{nl}{s}$). **(D)** Comparison between the measured death rates for conditioned media that was frozen and re-thawed and conditioned media that was directly used ($40 \frac{nl}{s}$, PEEK). **(E)** Distribution of the ages of the cultures used in this study. The data is based on 49 experiments from 9 platings. Every bar is based on data from at least 3 experiments from 2 different platings except for the static data in panel A and the PTFE data in panel C which are each based on 3 experiments from one plating. Asterisks that group several bars indicate statistical significance of an ANOVA test. Asterisks next to individual bars indicate statistical significance of a t-test between the leftmost condition and the condition at hand. *, **, ***, n.s indicate statistical significance at a level of confidence of 95%, 99%, 99.9% or <95%, respectively.

4.4 Chapter conclusion

In this chapter, we demonstrated a capacity for growing rat macrocultures (standard size) and microcultures in microfluidic devices. The observations made in sections 4.2.1.2 and 4.2.2 highlight the challenges that exists in the design of microfluidic devices for neuronal culture in finding a ‘goldilocks’ circulation regime. On one hand, enough nutrients and oxygen need to be allowed into the device to meet the requirements of the culture and, on the other hand, conditioning factors must be prevented from ‘escaping’ as they are required for sustaining the development. The precise design is strongly dependent on the size and density of the culture as these inform its oxygen and nutrient requirements and also the secretion rate of conditioning factors.

In the second part of this chapter we used a viability assay to quantitatively observe the health the cultures under flow. We found that using highly conditioned media can sustain the viability of the culture for several hours under flow and therefore consider it a promising approach for establishment of the system. Interestingly, the shear rate induced by the flow did not correlate with the viability which suggests that the deleterious effects are mediated solely by removal of conditioning factors and not at all by physical shear. Nevertheless, this is not the only possible interpretation for these results. A related study testing the viability of neuronal culture under a range of flow rates reported a shear threshold associated with culture degeneration [64]. This study found that a compound isolated from brain tissue named Galanin protects the cultures from the shear so, when it is introduced into the flow media, an effective increase in the degeneration threshold is observed. A possible interpretation of our results could therefore be that the conditioned media contains factors similar to Galanin that protect the cells from the shear and therefore effectively increase the flow rate threshold to a level exceeding the tested range. The study presented here cannot unambiguously distinguish the above-described narratives. This issue will be further addressed in the next chapter where electrophysiological measurements under flow will be presented and shed light on the mechanisms by which flow interacts with the culture.